Provided for non-commercial research and education use.
Not for reproduction, distribution or commercial use.


ISSN 0016-7037
Volume 75, Number 7
April 1, 2011

ELSEVIER

Geochimica et Cosmochimica Acta

JOURNAL OF THE GEOCHEMICAL SOCIETY AND THE METEORITICAL SOCIETY

Volume 75, Number 7 April 1, 2011

Articles

Continued on outside back cover

This article appeared in a journal published by Elsevier. The attached copy is furnished to the author for internal non-commercial research and education use, including for instruction at the authors institution and sharing with colleagues.

Other uses, including reproduction and distribution, or selling or licensing copies, or posting to personal, institutional or third party websites are prohibited.

In most cases authors are permitted to post their version of the article (e.g. in Word or Tex form) to their personal website or institutional repository. Authors requiring further information regarding Elsevier's archiving and manuscript policies are encouraged to visit:

http://www.elsevier.com/copyright

Author's personal copy

Available online at www.sciencedirect.com
ScienceDirect
Geochimica et Cosmochimica Acta 75 (2011) 1869–1888
Geochimica et Cosmochimica Acta
www.elsevier.com/locate/gca

U–Th systematics and ^{230}Th ages of carbonate chimneys at the Lost City Hydrothermal Field

Kristin A. Ludwig [a,*], Chuan-Chou Shen [b,*], Deborah S. Kelley [a], Hai Cheng [c], R. Lawrence Edwards [c]

[a] School of Oceanography, University of Washington, Seattle, WA, USA
[b] High-precision Mass Spectrometry and Environment Change Laboratory (HISPEC), Department of Geosciences, National Taiwan University, Taipei, Taiwan, ROC
[c] Department of Geology and Geophysics, University of Minnesota, Minneapolis, MN, USA

Received 2 June 2010; accepted in revised form 4 January 2011; available online 12 January 2011

Abstract

The Lost City Hydrothermal Field (LCHF) is a serpentinite-hosted vent field located 15 km west of the spreading axis of the Mid-Atlantic Ridge. In this study, uranium–thorium (U–Th) geochronological techniques have been used to examine the U–Th systematics of hydrothermal fluids and the ^{230}Th ages of hydrothermally-precipitated carbonate chimneys at the LCHF. Fluid sample analyses indicate that endmember fluids likely contain only 0.0073 ng/g U or less compared to 3.28 ± 0.03 ng/g of U in ambient seawater. For fluid samples containing only 2–21% ambient seawater (1.1–11 mmol/kg Mg), Th concentration is 0.11–0.13 pg/g and surrounding seawater concentrations average 0.133 ± 0.016 pg/g. The ^{230}Th/^{232}Th atomic ratios of the vent fluids range from $1\ (\pm 10) \times 10^{-6}$ to $11\ (\pm 5) \times 10^{-6}$, are less than those of seawater, and indicate that the vent fluids may contribute a minor amount of non-radiogenic ^{230}Th to the LCHF carbonate chimney deposits. Chimney ^{238}U concentrations range from 1 to 10 μg/g and the average chimney corrected initial δ^{234}U is 147.2 ± 0.8, which is not significantly different from the ambient seawater value of 146.5 ± 0.6. Carbonate ^{232}Th concentrations range broadly from 0.0038 ± 0.0003 to 125 ± 16 ng/g and ^{230}Th/^{232}Th atomic ratios vary from near seawater values of $43\ (\pm 8) \times 10^{-6}$ up to $530\ (\pm 25) \times 10^{-3}$. Chimney ages, corrected for initial ^{230}Th, range from 17 ± 6 yrs to 120 ± 13 kyrs. The youngest chimneys are at the intersection of two active, steeply-dipping normal faults that cut the Atlantis Massif; the oldest chimneys are located in the southwest portion of the field. Vent deposits on a steep, fault-bounded wall on the east side of the field are all <4 kyrs old, indicating that mass wasting in this region is relatively recent. Comparison of results to prior age-dating investigations of submarine hydrothermal systems shows that the LCHF is the most long-lived hydrothermal system known to date. It is likely that seismic activity and active faulting within the Atlantis Massif and the Atlantis Fracture Zone, coupled with volumetric expansion of the underlying serpentinized host rocks play major roles in sustaining hydrothermal activity at this site. The longevity of venting at the LCHF may have implications for ecological succession of microorganisms within serpentinite-hosted vent environments.
© 2011 Elsevier Ltd. All rights reserved.

1. INTRODUCTION

The Lost City Hydrothermal Field (LCHF) is a serpentinite-hosted hydrothermal system located 15 km west of the spreading axis of the Mid-Atlantic Ridge (MAR) (Kelley et al., 2001, 2005). Carbonate chimneys within the field are the tallest known hydrothermal edifices in a marine

* Corresponding authors. Tel.: +1 206 293 5384 (K.A. Ludwig). Present address: Consortium for Ocean Leadership, Washington, DC, USA. Tel.: +886 2 3366 5878; fax: +886 2 3365 1917 (C.-C. Shen).
E-mail addresses: kristin.a.ludwig@gmail.com (K.A. Ludwig), river@ntu.edu.tw (C.-C. Shen).

0016-7037/$ - see front matter © 2011 Elsevier Ltd. All rights reserved.
doi:10.1016/j.gca.2011.01.008

Author's personal copy

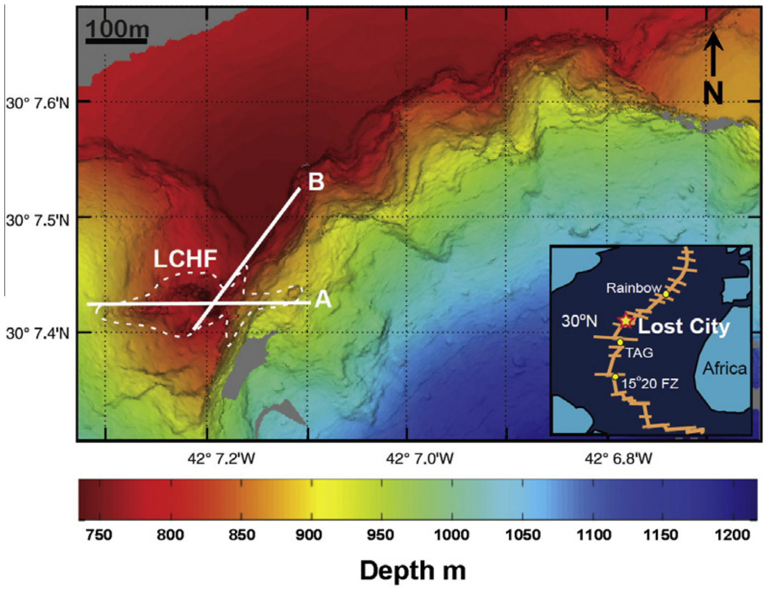

Fig. 1. Location map with tectonic faults. The LCHF is located at 30°N, 15 km west of the spreading axis of the Mid-Atlantic Ridge (see inset). The field is at a depth of ~750 m atop an oceanic core complex called the Atlantis Massif. The Atlantis Transform Fault bounds the southern end of the field ~20 m to the south at a depth of ~5000 m, and the eastern side of the field is bounded by a steep escarpment created by mass wasting. Two steeply-dipping normal faults striking east–west (Fault A) and ~020° (Fault B) focus fluid flow. The vent field occupies an area of ~500 m^2 (outline). (modified from Karson et al. (2006)).

environment, rising up to 60 m above the seafloor (Fig. 1). Discovered in 2000, the unique geologic setting and chemistry of the LCHF has renewed debates on the amount and source of heat required to establish and sustain off-axis hydrothermal circulation in systems where active serpentinization is ongoing in the underlying rocks (e.g., Macdonald and Fyfe, 1985; Kelley et al., 2001, 2005; Lowell and Rona, 2002; Früh-Green et al., 2003; Allen and Seyfried, 2004; Emmanuel and Berkowitz, 2006). Unlike magmatically-fuelled black smoker systems, hydrothermal circulation at the LCHF is believed to be driven by both residual crustal heat in the underlying mantle and lesser gabbroic rocks and in part by subsurface serpentinization reactions (Kelley et al., 2001, 2005; Früh-Green et al., 2003), although Allen and Seyfried (2004) argue that an off-axis magmatic heat source several kilometers to the east likely drives hydrothermal circulation. Even though the LCHF heat source remains poorly understood, the immense size of the chimneys and the ~500 m^2 aerial extent of the field indicate that it is a long-lived system (Früh-Green et al., 2003; Kelley et al., 2005). Previous studies have shown that fluid flow within the field is channeled by the intersection of two major faults, one which is subparallel to the nearby east-west trending Atlantis Transform Fault and another which strikes at ~020° (Kelley et al., 2005; Karson et al., 2006) (Fig. 1). Volume expansion during serpentinization within the basement rocks likely promotes cracking and hydrothermal circulation within the field and contributes to maintaining long-lived fluid flow paths (Kelley et al., 2001, 2005; Früh-Green et al., 2003; Boschi et al., 2006; Karson et al., 2006).

Despite multiple studies of the geologic history of the Atlantis Massif (Cann et al., 1997; Blackman et al., 1998, 2002; Schroeder and John, 2004; Canales et al., 2004; Expedition Scientific Party, 2005; Boschi et al., 2006), numerous questions remain concerning the development, formation conditions, and duration of hydrothermal activity within this novel hydrothermal system. Previous work using radiocarbon techniques shows that hydrothermal activity has been on-going for at least 30 kyrs, yet modeling suggests that the field may be even older (Früh-Green et al., 2003). The nearly monomineralic carbonate mineralogy of the LCHF chimneys (Kelley et al., 2005; Ludwig et al., 2006) is amenable to both radiocarbon and U-series dating, allowing important constraints to be placed on the history of hydrothermal activity and tectonism within the field and the timescales over which the chimneys form. Uranium–thorium (^{238}U–^{234}U–^{230}Th–^{232}Th or U–Th or ^{230}Th) disequilibrium dating is a powerful geochronological tool used to date inorganic and biogenic materials ranging in age from modern to 600 kyrs (e.g., Edwards et al., 1986/1987, 1987, 2003; Stirling et al., 2001; Thompson et al., 2003; Andersen et al., 2008; Shen et al., 2008). This comprehensive study presents the first U–Th analyses of alkaline fluids and carbonate deposits from the LCHF. Analyses of six vent fluid, five seawater, and over 60 discrete chimney structures provide new insights into the behavior of U and Th in marine hydrothermal environments where serpentinization is a major on-going process and into chimney development within the LCHF. Techniques used in this study may be applied to examining the age and tectonic history of other hydrothermal environments where carbonate is routinely precipitated including ophiolite springs, tufas, methane hydrates, and methane seeps.

Author's personal copy

2. GEOLOGIC SETTING AND FLUID CHEMISTRY OF THE LCHF

The LCHF is located at a depth of ~750 m (Fig. 1). Unlike most hydrothermal vent fields known to date that are characterized by axial, basalt-hosted sulfide structures, the LCHF is west of the MAR spreading axis on an oceanic core complex called the Atlantis Massif (Kelley et al., 2001). The massif is composed of 1–2 Myr-old variably serpentinized peridotite with lesser altered and deformed gabbroic material: the flat summit of the massif is capped by a ~1 m thick layer of hydrothermally-cemented carbonate ooze (Kelley et al., 2001, 2005; Blackman et al., 2002; Früh-Green et al., 2003; Karson et al., 2006) (Figs. 1 and 2). The field is perched on a down-dropped bench on the southern face of the massif, where large (up to 60 m tall) carbonate chimneys are the hallmark of the venting system (Fig. 2) (Kelley et al., 2001, 2005). These deposits form during mixing of warm (<40–91 °C), diffusely venting hydrothermal fluids and surrounding seawater (Kelley et al., 2001, 2005; Ludwig et al., 2006). The chimneys are composed of aragonite, calcite, and brucite and evolve from small, nascent fracture-filling deposits to large complex pinnacles >30 m tall and 100 m across (Kelley et al., 2001, 2005; Ludwig et al., 2006). Actively venting, porous (up to 50%) carbonate deposits and the effusing warm fluids provide a rich habitat for diverse microbial communities of Archaea and bacteria and a macrofaunal community that includes amphipods, gastropods, and mussels (Schrenk et al., 2003; Kelley et al., 2005; Brazelton et al., 2006, 2010). Inactive, well-lithified chimneys are home to deep sea corals, crabs, and serpulid worms (Kelley et al., 2005).

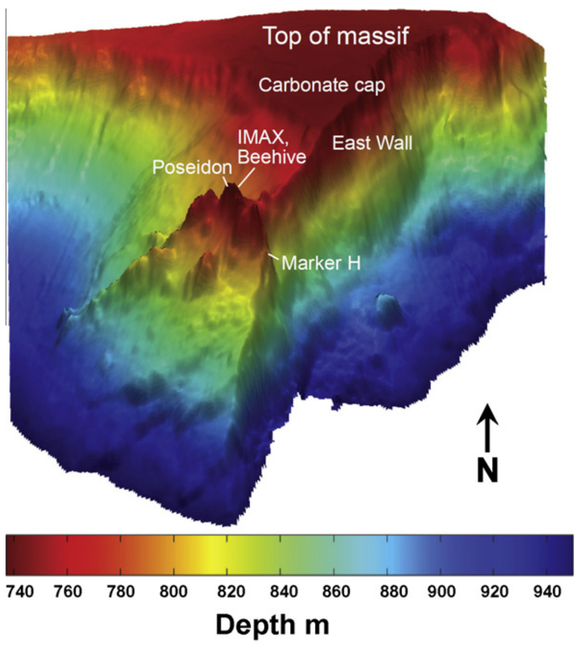

Fig. 2. Bathymetry of the LCHF. Present day hydrothermal activity at the LCHF is concentrated on a down-dropped bench on the southern edge of the massif and along the steep East Wall immediately beneath the summit. The tallest structure at the LCHF is the Poseidon complex, which rises 60 m from the seafloor. Other features in the field include the IMAX and Beehive chimneys which are parasitic structures on the north side of Poseidon, and Marker H which denotes the eastern-most extent of active vent chimneys. The distinctively flat top of the massif is capped by a layer of ~1 m thick well-lithified deposit of carbonate ooze.

Subsurface serpentinization reactions at the LCHF produce particle-free, high pH (9–11), low metal, low silica fluids that contain high concentrations of calcium (up to ~30 mmol/kg), and abiogenically-produced H_2 (<1–15 mmol/kg), CH_4 (1–2 mmol/kg), and low molecular weight hydrocarbons; they are nearly void of CO_2 (Kelley et al., 2005; Proskurowski et al., 2006, 2008). Similar to black smoker systems, magnesium (Mg) is removed during hydrothermal circulation and the hottest fluid samples (91 °C) contain <1 mmol/kg Mg (Kelley et al., 2005).

3. U–Th SYSTEMATICS AND GEOCHRONOLOGY

3.1. ^{230}Th dating theory and initial ^{230}Th

U–Th techniques have been particularly successful for precise dating of corals and speleothems (e.g., Edwards et al., 1987, 2003; Cheng et al., 1998, 2000a; Goldstein and Stirling, 2003; Branchu et al., 2005; Shen et al., 2008, 2010). Assuming that there is no further loss or gain of U or Th, the ^{230}Th age is determined by the radiogenic ingrowth of ^{234}U and ^{230}Th using the age equation below (after Kaufman and Broecker, 1965 and Edwards et al., 2003):

$$\left(\frac{^{230}\mathrm{Th}}{^{238}\mathrm{U}}\right)_m = 1 + \left(\left(\frac{^{232}\mathrm{Th}}{^{238}\mathrm{U}}\right)_m\left(\frac{^{230}\mathrm{Th}}{^{232}\mathrm{Th}}\right)_{nr} - 1\right)e^{\lambda_{230}t} + \frac{\delta^{234}\mathrm{U}_m}{1000}\left[\frac{\lambda_{230}}{\lambda_{230}-\lambda_{234}}\right]\left(1-e^{(\lambda_{234}-\lambda_{230})t}\right) \quad (1)$$

In this equation, all isotope ratios are activity ratios, m denotes measured quantities, nr denotes non-radiogenic, and λ_{230} and λ_{234} are the decay constants of ^{230}Th and ^{234}U, respectively (values from Cheng et al., 2000b). The $^{234}U/^{238}U$ ratio must be measured and appears explicitly as a term in the age equation. The $^{234}U/^{238}U$ ratio is expressed in δ-notation, where

$$\delta^{234}\mathrm{U}_m = \left[(^{234}\mathrm{U}/^{238}\mathrm{U})_m/(^{234}\mathrm{U}/^{238}\mathrm{U})_{eq} - 1\right] \times 1000 \quad (2)$$

and

$$\delta^{234}\mathrm{U}_{initial} = \delta^{234}\mathrm{U}_m \times e^{\lambda_{234}t} \quad (3)$$

The ratio $(^{234}U/^{238}U)_{eq}$ is the activity ratio of $^{234}U/^{238}U$ at secular equilibrium (which equals 1) (Edwards et al., 1986/1987). The initial δ^{234}U ($\delta^{234}U_{initial}$) refers to the initial deviation of ^{234}U from secular equilibrium and is calculated from the measured δ^{234}U ($\delta^{234}U_m$) and the non-radiogenic ^{230}Th ($^{230}Th_{nr}$)-corrected age. The two unknowns in Eq. (1) are $^{230}Th_{nr}$, which is the amount of non-radiogenic ^{230}Th, and t, which is the ^{230}Th age in years.

With high precision mass spectrometric techniques (Edwards et al., 1986/1987; Stirling et al., 2001; Shen et al., 2002, 2006; Andersen et al., 2008), the ability to achieve accurate ^{230}Th ages relies on precise determination

Author's personal copy

of the amount of $^{230}Th_{nr}$ (e.g., Edwards et al., 1986/1987, 2003; Edwards, 1988; Cheng et al., 2000a; Dorale et al., 2001; Shen et al., 2008). $^{230}Th_{nr}$ can be introduced to carbonate matrices via any combination of "external" sources, such as seawater and detritus, and "internal" processes, such as diagenesis and α-recoil (e.g., Edwards, 1988; Cobb et al., 2003; Robinson et al., 2004; Shen et al., 2008). For coral studies, $^{230}Th_{nr}$ is typically assessed by constructing isochrons from growth bands and/or directly measuring the $^{230}Th/^{232}Th$ atomic ratio of ambient seawater (e.g., Chen et al., 1986a; Edwards et al., 2003; Shen et al., 2008). The ^{230}Th ages are then corrected to the $^{230}Th_{nr}$ during off-line data correction (Cheng et al., 2000b; Shen et al., 2002).

In hydrothermal and seep environments, vent fluids pose a potential additional source of $^{230}Th_{nr}$ to mineral precipitates. However, only a few studies have analyzed U and Th isotopic composition in co-registered samples of fluids and hydrothermal deposits. Michard and Albarede (1985) analyzed vent fluids from the East Pacific Rise (EPR) and were the first to show that U is removed from seawater during hydrothermal circulation. Chen et al. (1986b) examined the U–Th–Pb systematics of hydrothermal fluids egressing from black smoker chimneys at 21°N on the EPR and in the Guaymas Basin. They confirmed Michard and Albarede's (1985) results and showed that the concentration of ^{232}Th in hydrothermal fluids (up to 4.3 pg/g) was elevated compared to ambient seawater (0.004–0.037 pg/g). Similarly, Anderson et al. (1982) and Simpson et al. (1982) attributed high concentrations of Th in spring fluids in Mono Lake, California, to an enhanced solubility of Th when complexed with carbonate ions. These results indicate that vent and spring fluids can be an additional source of $^{230}Th_{nr}$ to mineral deposits, which must be assessed for accurately correcting the U–Th ages of hydrothermal chimneys.

3.2. U–Th systematics in hydrothermal environments

Very little work has been done to investigate U–Th systematics and ages in hydrothermal deposits. In mid-ocean ridge systems, Lalou and others have successfully employed α-counting and thermal ionization mass spectrometry (TIMS) techniques to date sulfide deposits from the Trans-Atlantic Geotraverse (TAG), Snake Pit, and 14°45′N sites on the MAR and the MESO Zone (after the German research vessels R/V *MEteor* and R/V *SOnne*, located in the central part of the 85 km-long fourth ridge segment at about 23°23.50′S, 69°14.50′E on the Central Indian Ridge) (Lalou and Brichet, 1982; Lalou et al., 1993, 1996, 1998a, 1998b). A study by You and Bickle (1998) complemented Lalou's work at TAG and correlated ^{230}Th ages of sulfides from ODP core samples (ODP Leg 158) with mound stratigraphy established by Humphris et al. (1995). This work resulted in one of the first growth-age models of any submarine hydrothermal system and established TAG as one of the longest-lived active vent fields known with a maximum age of 50 kyrs. In both studies, initial ^{230}Th in the sulfides was assumed to be negligible. Münch et al. (2001) employed ^{230}Th ages of sulfide deposits to construct a chronology of the Mt. Jourdanne field on the Southwest Indian Ridge and found a maximum age of 70 kyrs. Although limited in number compared to the applications of U-series techniques to corals and speleothems, these studies provide a foundation for further examination of U–Th systematics in hydrothermal environments.

4. METHODS

4.1. Sample collection

4.1.1. Vent fluids and seawater

A total of six vent fluid and five seawater samples were collected during the 2003 and 2005 expeditions to the LCHF (Table 1). In 2003, vent fluid samples were collected using the Deep Submergence Vehicle (DSV) *ALVIN* with titanium major bottles that were manually cleaned with deionized water prior to deployment. In 2005, seawater samples were collected from 745 m during CTD casts on the R/V Ronald Brown. In 2005, vent fluid samples were collected using the remotely operated vehicle (ROV) *Hercules* and titanium major bottles. During the 2005 expedition, major samplers were manually cleaned, then rinsed with 1.5 N HNO_3 and deionized water prior to deployment to minimize Th contamination from one sample to the next. During both expeditions, fluid samples were collected on different days from different vents. Aliquots (50–300 ml) of vent fluid samples were transferred to acid-cleaned HDPE plastic bottles. None of the samples were filtered. All samples were acidified with 4 N HNO_3. Vent fluid temperatures were measured using the temperature probe of DSV *ALVIN* and ROV *Hercules* or a probe mounted on the vent fluid sampling bottles.

4.1.2. Chimneys

Over 150 chimney samples of LCHF carbonate deposits have been collected using the DSV *ALVIN* and ROV *Hercules* during the 2000, 2003, and 2005 expeditions to the LCHF. In this study, 67 chimney samples were selected for age dating analysis based on their location in the field.

LCHF carbonate deposits are classified into three categories based on field observations: "active" (structures with actively venting fluid and/or structures with measured temperatures above ambient seawater temperature), "inactive" (chimneys that were not visibly emitting fluid), and "fissure" deposits, which are carbonate deposits growing directly from cracks in the basement or cap rock. Samples collected from the carbonate cap are categorized separately as "cap" samples. These classifications are described in detail in Ludwig et al. (2006) and example morphologies are shown in Figure EA-1 (see Electronic annex). The active chimneys are typically much more friable than the inactive deposits and therefore much easier to collect, which biases sample collection. Several samples were recovered from talus ramps and this is noted in the data tables and figures. A total of 21 active, 3 cap, 11 fissure, and 32 inactive structures were analyzed. Six samples were analyzed twice (different powders from the same chimney) and are denoted with "a" and "b" in their sample identification number.

After recovery, all carbonate samples were dried onboard the vessel and stored in plastic bags. For U–Th shore-based analyses, chimney subsamples were lightly

Author's personal copy

Table 1
Seawater and fluid isotope chemistry.

Sample ID[a]	Collection year	Site	Depth (m)	Temperature °C)[b]	Sample mass (g)[c]	Mg (mmol/kg)[d]	Est.% vent fluid[e]	^{238}U (ng/g)	^{232}Th (pg/g)	δ^{254}U measured[f]	[^{230}Th/^{138}U] activity[g]	[^{230}Th/^{232} Th] $\times 10^{-6}$[h]
Seawater												
SW-2	2005	Ambient seawater	745	10.6	529.87	54.50	0	3.2860 ± 0.0027	0.1421 ± 0.0013	146.9 ± 1.4	0.0001046 ± 0.0000088	39.9 ± 3.4
SW-3	2005	Ambient seawater	745	10.6	513.62	54.50	0	3.2835 ± 0.0031	0.1263 ± 0.0014	146.1 ± 1.5	0.0001129 ± 0.0000060	48.4 ± 2.6
SW-4	2005	Ambient seawater	745	10.6	525.42	54.50	0	3.2827 ± 0.0022	0.1373 ± 0.0014	146.4 ± 1.3	0.0001117 ± 0.0000055	44.1 ± 2.2
SW-5	2005	Ambient seawater	745	10.6	527.19	54.50	0	3.2839 ± 0.0026	0.1256 ± 0.0013	146.6 ± 1.3	0.0001078 ± 0.0000054	46.5 ± 2.4
H08_080105_M3_0246	2005	Ambient seawater, top of cap	759	~10	54.27	53.64	2	3.2456 ± 0.0034	0.443 ± 0.013	146.5 ± 1.5	0.000289 ± 0.000058	35.0 ± 7.1
Vent fluids												
H02_072605_M1_0443	2005	Marker H	841	41	137.10	49.95	8	3.124 ± 0.015	2.196 ± 0.012	151.2 ± 9.3	0.002320 ± 0.000074	54.5 ± 1.7
H03 072705_M3_0354	2005	Marker 3	732	88	114.15	44.36	19	2.891 ± 0.013	1.863 ± 0.021	139.1 ± 9.3	0.00408 ± 0.00021	104.6 ± 5.4
H04_072805_M1_0416	2005	Marker H	843	63.5	203.06	1.08	98	0.0328 ± 0.0012	0.1239 ± 0.0036	154 ± 31	0.0024 ± 0.0011	10.7 ± 4.7
H06_073005_M4_0413	2005	Beehive	742	91	100.79	1.14	98	0.00734 ± 0.00089	0.1115 ± 0.0070	92 ± 116	0.0007 ± 0.0095	1 ± 10
H07_073105_M2_1238	2005	Marker 6	777	44	98.51	48.32	11	2.280 ± 0.045	2.775 ± 0.034	183 ± 46	0.00244 ± 0.00020	33.1 ± 2.7
3863m15	2003	Marker 3	731	81	293.72	11.30	79	0.5373 ± 0.0017	0.1264 ± 0.0026	147.9 ± 2.6	0.000364 ± 0.000057	25.6 ± 4.0

Samples from the 2005 expedition are labeled as a dive number-date-major sample #-time stamp naming convention. For example, sample number H07_073105_M2_1238 was collected during ROV *Hercules* Dive 7 on July 31, 2005 using major sampler 2 at 12:38 (GMT).

[a] Seawater ("SW-X") samples collected using CTD, all other samples collected using titanium major bottles. Sample 3863m15 was collected during ALVIN Dive #3863 using major sampler #15.

[b] Seawater temperature measured by CTD; vent fluid temperatures measured using temperature probe.

[c] Sample mass used for U–Th isotopic analysis.

[d] Mg concentration, provided by D. Butterfield, NOAA-PMEL, with a 2σ error of 2%.

[e] Determined from Mg concentration, based on zero Mg endmember.

[f] $\delta^{234}U = ([^{234}U/^{238}U]_{activity} - 1) \times 1000$.

[g] Calculated activity ratio based on decay constant values $9.1577 \times 10\ yr^{-1}$ for ^{230}Th, $2.8263 \times 10^{-6}\ yr^{-1}$ for ^{234}U (Cheng et al., 2000b), and $1.55125 \times 10^{-10}\ yr^{-1}$ for ^{238}U (Jaffey et al., 1971).

[h] This is the atomic ratio of ^{230}Th/^{232}Th.

Author's personal copy

Table 2
U and Th data and ^{230}Th ages for Lost City carbonate chimney samples[#].

Sample ID	Sample type	Sample location	Temperature (°C)	^{238}U (ng/g)	^{232}Th (pg/g)	δ^{234}U measured[a]	[^{230}Th/^{238}U] activity[b]	[^{230}Th/^{232}Th] 10^{-6c}	Age uncorrected	Age corrected[d]	$\delta^{234}U_{initial}$, corrected[e]
Active samples											
3651-1022	Active	Poseidon (Marker 3)	75	2820.0 ± 5.4	884.4 ± 2.7	149.2 ± 1.6	0.001406 ± 0.000025	74.0 ± 1.3	133.7 ± 2.4	43 ± 90	149.2 ± 1.6
3651-1149	Active	Poseidon (Marker 3)	55	3775.4 ± 8.7	1047.6 ± 9.5	148.8 ± 1.8	0.001677 ± 0.000034	99.8 ± 2.2	159.5 ± 3.2	80 ± 80	148.8 ± 1.8
3862-1219	Active	Poseidon (Marker 3)	59	3613.3 ± 9.5	586.3 ± 9.2	145.9 ± 1.9	0.003350 ± 0.000032	340.9 ± 6.2	319.7 ± 3.1	273 ± 47	146.0 ± 1.9
3862-1325	Active	Poseidon (Marker 3), South spire	59	2356.3 ± 3.3	468 ± 26	148.0 ± 1.8	0.000939 ± 0.000046	78.1 ± 5.7	89.4 ± 4.4	32 ± 58	148.0 ± 1.8
3864-1524	Active	IMAX flange edge, front side	53.5	5049 ± 11	1433 ± 12	148.0 ± 1.5	0.002094 ± 0.000023	121.8 ± 1.7	199.3 ± 2.3	118 ± 82	148.0 ± 1.5
3864-1537	Active	IMAX flange edge, left side	53.5	3720.2 ± 4.9	42.7 ± 4.2	144.8 ± 1.9	0.000218 ± 0.000059	314 ± 90	20.8 ± 5.6	17.5 ± 6.5	144.8 ± 1.9
3867-1225	Active	Spire near Marker 7		5630.8 ± 9.1	152.9 ± 7.3	145.0 ± 1.8	0.000484 ± 0.000052	294 ± 34	46.1 ± 4.9	38.3 ± 9.3	145.0 ± 1.8
3869-1404	Active	Marker C, flange	9.3	5214.4 ± 8.4	98 ± 17	145.0 ± 1.9	0.00051 ± 0.00024	446 ± 223	48 ± 23	43 ± 23	145.0 ± 1.9
3869-1443	Active	Marker C, spire	9.4	6300 ± 19	1248 ± 10	147.6 ± 1.7	0.001947 ± 0.000023	162.3 ± 2.3	185.5 ± 2.2	128 ± 57	147.6 ± 1.7
3869-1446	Active	Marker C, flange	9.4	3669.6 ± 4.8	1375 ± 19	147.4 ± 1.8	0.00489 ± 0.00013	215.5 ± 6.4	467 ± 12	359 ± 109	147.5 ± 1.8
3876-1104a	Active	Spire east of Marker H	12.5	2414.9 ± 4.9	118.9 ± 4.6	147.4 ± 2.2	0.001249 ± 0.000092	419 ± 35	118.9 ± 8.8	105 ± 17	147.5 ± 2.2
3876-1104b	Active	Spire east of Marker H	12.5	2562.8 ± 3.5	148.7 ± 4.0	144.8 ± 1.6	0.001575 ± 0.000076	448 ± 25	150.3 ± 7.2	134 ± 18	144.8 ± 1.6
3876-1436	Active	Beehive chimney, N side of Poseidon	90.7	3177.8± 4.4	676 ± 22	148.6 ± 2.2	0.001174 ± 0.000034	91.2 ± 4.0	111.7 ± 3.2	50 ± 61	148.6 ± 2.2
3877-1606	Active	Small chimney near Marker H	25/62	2789.4 ± 5.1	363.6 ± 9.1	147.1 ± 1.6	0.000919 ± 0.000018	116.5 ± 3.7	87.6 ± 1.7	50 ± 38	147.1 ± 1.6
3880-1532	Active	Structure below Marker H		2936.9 ± 4.0	439 ± 22	146.6 ± 1.8	0.000849 ± 0.000035	93.8 ± 6.1	80.9 ± 3.4	38 ± 43	146.7 ± 1.8
3881-1202	Active	Flange near Marker H	54.5	2748.5 ± 3.5	37.9 ± 3.4	142.9 ± 1.6	0.000259 ± 0.000027	310 ± 43	24.8 ± 2.6	20.8 ± 4.8	142.9 ± 1.6
3881-1408	Active	Top of Poseidon (Marker 3)	36/73	2149.6 ± 3.4	53.8 ± 3.6	143.9 ± 2.0	0.000433 ± 0.000038	286 ± 32	41.4 ± 3.6	34.1 ± 8.1	143.9 ± 2.0
H04-072805-R0325	Active	Friable chimney from near top of Marker H	63.5	3156.6 ± 4.2	64.3 ± 4.5	147.3 ± 1.9	0.000403 ± 0.000079	326 ± 68	38.3 ± 7.5	32.5 ± 9.5	147.4 ± 1.9
H06-073005-R0316_a	Active	Beehive chimney, N side of Poseidon	91	3155.8 ± 5.0	78.2 ± 4.5	145.3 ± 2.0	0.000558 ± 0.000040	372 ± 34	53.3 ± 3.8	46.1 ± 8.1	145.3 ± 2.0
H06-073005-R0316_b	Active	Beehive chimney, N side of Poseidon	91	3409.1 ± 6.8	98.7 ± 7.9	143.6 ± 2.3	0.000444 ± 0.000050	253 ± 35	42.4 ± 4.8	34.0 ± 9.7	143.6 ± 2.3
H06-073005-R0843	Active	Venting chimlet near Marker 6		4471.9 ± 7.3	161.5 ± 4.1	147.3± 1.9	0.000909 ± 0.000042	415 ± 22	86.5 ± 4.0	76 ± 11	147.3± 1.9
H07-073105-R1053	Active	Chimney at Marker 6	44	4755 ± 10	8,954 ± 380	144.7 ± 2.2	0.0551 ± 0.0015	483 ± 24	5384 ± 153	4840 ± 567	146.7 ± 2.3
H08-073105-R2238	Active	Venting from crack in top of cap		3006.9 ± 4.6	121.2 ± 3.7	147.5 ± 1.9	0.000668 ± 0.000056	274 ± 24	63.6 ± 5.3	52 ± 13	147.5 ± 1.9
Carbonate cap samples											
3862-1549	Cap	Carbonate cap		3582.6 ± 6.2	88,092 ± 10314	145.1 ± 2.2	0.425 ± 0.022	286 ± 37	50,129 ± 3297	42,920 ± 8135	163.8 ± 4.4
3867-1121	Cap	Talus of carbonate cap		453.98 ± 0.63	84,665 ± 10459	187.0 ± 2.1	0.485 ± 0.064	43.0 ± 7.8	Not determinable	Not determinable	Not determinable
3867-1123	Cap	Carbonate cap		1284.2 ± 1.9	127,318 ± 16939	145.6 ± 2.0	0.671 ± 0.042	112 ± 16	93,939 ± 9174	61,911 ± 40227	173 ± 17
Fissure samples											
3651-0944	Fissure	Poseidon (Marker 3)		2806.9 ± 3.7	2804 ± 26	149.8 ± 1.7	0.00790 ± 0.00012	130.5 ± 2.3	752 ± 12	465 ± 288	150.0 ± 1.7
3862-1659	Fissure	Marker 4		2792.3 ± 2.7	16,959 ± 72	146.1 ± 1.5	0.04330 ± 0.00052	117.7 ± 1.5	4202 ± 52	2437 ± 1780	147.1 ± 1.7
3863-1551	Fissure	East wall, growing from massive carbonate		2273.6 ± 3.2	2598 ± 24	149.6 ± 1.7	0.01163 ± 0.00020	168.0 ± 3.3	1110 ± 20	781 ± 330	149.9 ± 1.7
3865-1322	Fissure	Growing from crack in top of cap		2507.1 ± 3.8	7290 ± 33	147.6 ± 1.8	0.01982 ± 0.00020	112.5 ± 1.2	1902 ± 20	1061 ± 844	148.0 ± 1.9
3876-1219	Fissure	East wall		2254.2 ± 2.7	3698 ± 23	146.7 ± 1.7	0.01287 ± 0.00016	129.5 ± 1.8	1232 ± 15	758 ± 475	147.0 ± 1.7
3879-1258	Fissure	North of Poseidon		3042.0 ± 3.7	6694 ± 26	146.5 ± 1.8	0.02957 ± 0.00023	221.9 ± 1.9	2852 ± 23	2216 ± 638	147.4 ± 1.8
3880-1353	Fissure	Southwest of Marker 7		5811.0 ± 7.3	43,100 ± 196	148.1 ± 1.5	0.05566 ± 0.00055	123.9 ± 1.3	5,421 ± 55	3267 ± 2177	149.5 ± 1.8
Inactive samples											
3651-0938a	Inactive	Poseidon		10,497 ± 16	12,021 ± 290	124.2 ± 1.9	0.2088 ± 0.0020	3011 ± 78	22,356 ± 245	22,021 ± 415	132.2 ± 2.0
3651-0938b	Inactive	Poseidon		10,203 ± 14	74,883 ± 368	127.2 ± 1.6	0.3687 ± 0.0023	829.5 ± 6.4	42,906 ± 331	40,762 ± 2190	142.8 ± 2.0
3651-1123	Inactive	Poseidon		5510.4 ± 7.8	14,920 ± 55	149.3 ± 1.8	0.02641 ± 0.00025	161.1 ± 1.6	2537 ± 25	1756 ± 784	150.1 ± 1.8
3651-1231a	Inactive	Poseidon		5034.4 ± 6.1	22,056 ± 107	146.6 ± 1.7	0.02654 ± 0.00037	100.0 ± 1.5	2556 ± 36	1286 ± 1278	147.2 ± 1.7
3651-1231b	Inactive	Poseidon		4652.1 ± 7.4	6559 ± 165	148.0 ± 2.0	0.02694 ± 0.00056	316 ± 10	2592 ± 55	2186 ± 411	148.9 ± 2.0
3862-1432	Inactive	Tower near Marker 6		3574.5 ± 5.4	4842 ± 190	143.8 ± 1.7	0.02975 ± 0.00070	363 ± 17	2876 ± 68	2484 ± 399	144.8 ± 1.7
3862-1517base	Inactive	Tower near Marker 6		4734.3 ± 6.2	21,486 ± 91	145.7 ± 1.9	0.02410 ± 0.00035	87.7 ± 1.3	2320 ± 34	1003 ± 1326	146.2 ± 2.0
3862-1517top	Inactive	Tower near Marker 6		3967.9 ± 4.8	18,201 ± 101	147.4 ± 1.6	0.02345 ± 0.00034	84.4 ± 1.3	2254 ± 34	925 ± 1338	147.7 ± 1.7

Author's personal copy

3862-1530	Inactive	Near Marker 6	2575.6 ± 4.2	601 ± 10	145.0 ± 1.9	0.00923 ± 0.00014	654 ± 15	884 ± 13	817 ± 69	145.3 ± 1.9
3864-1647	Inactive	Chimney near Poseidon (Marker 1)	6345.9 ± 8.6	70,204 ± 473	148.1 ± 1.6	0.0794 ± 0.0010	118.5 ± 1.7	7812 ± 103	4,585 ± 3279	150.0 ± 2.2
3867-1228	Inactive	Spire near Marker 7	6282.7 ± 7.9	965 ± 18	142.1 ± 1.4	0.003759 ± 0.000083	404 ± 12	359.9 ± 8.0	315 ± 45	142.2 ± 1.4
3867-1308	Inactive	Spire below Poseidon	5002.8 ± 6.6	67,626 ± 1004	148.0 ± 1.6	0.1390 ± 0.0032	169.8 ± 4.6	14055 ± 342	10,109 ± 4038	152.3 ± 2.4
3871-1442	Inactive	Fallen carbonate near Marker 2	1843.7 ± 2.0	617 ± 10	146.4 ± 1.7	0.01207 ± 0.00020	596 ± 14	1155 ± 19	1059 ± 98	146.9 ± 1.7
3871-1512	Inactive	SW of field	3673.6 ± 4.1	46,471 ± 250	144.3 ± 1.7	0.1894 ± 0.0017	247.2 ± 2.6	19,683 ± 198	15,989 ± 3766	151.0 ± 2.4
3872-1530	Inactive	Marble talus at base of field	4786.1 ± 5.5	9143 ± 32	104.3 ± 1.6	0.7106 ± 0.0020	6,142 ± 27	110,038 ± 604	109,484 ± 818	142.1 ± 2.2
3872-1544a	Inactive	Spire near southwest edge of field	4393.3 ± 5.8	97,269 ± 8547	105.9 ± 1.5	0.903 ± 0.028	674 ± 63	175,946 ± 13221	169,516 ± 14167	170.9 ± 7.6
3872-1544b	Inactive	Spire near southwest edge of field	4579.3 ± 6.3	82,130 ± 12809	108.2 ± 1.6	0.768 ± 0.040	707 ± 116	125,366 ± 11910	120,097 ± 12620	151.9 ± 6.2
3873-1233	Inactive	Talus from west of main field	345.3 ± 1.0	54,506 ± 3929	115.8 ± 6.6	3.32 ± 0.11	347 ± 27	Not determinable	Not determinable	Not determinable
3876-1113	Inactive	Inactive spire below and east of Marker H	2060.1 ± 2.5	7864 ± 30	147.1 ± 1.8	0.03229 ± 0.00029	139.7 ± 1.4	3116 ± 29	2011 ± 1111	148.0 ± 1.8
3876-1133	Inactive	Spire near Marker 7	2233.4 ± 3.2	1459 ± 154	145.3 ± 1.8	0.0149 ± 0.0018	377 ± 60	1430 ± 173	1242 ± 256	145.8 ± 1.8
3877-1501	Inactive	Lower southeast corner of field	1136.6 ± 2.5	124,690 ± 15623	122.2 ± 2.4	2.86 ± 0.12	430 ± 57	Not determinable	Not determinable	Not determinable
3880-1557	Inactive	Spire from southeast side of field	1795.7 ± 2.3	7623 ± 239	146.4 ± 1.6	0.1220 ± 0.0018	475 ± 16	12,262 ± 192	11,036 ± 1249	151.1 ± 1.8
3881-1228	Inactive	Spire near Marker H	3660.6 ± 5.8	84.4 ± 3.4	145.0 ± 1.8	0.000568 ± 0.000025	407 ± 24	54.2 ± 2.3	47.6 ± 7.1	145.1 ± 1.8
3881-1256a	Inactive	Spire near Marker H	3267.4 ± 5.5	107.3 ± 4.0	146.4 ± 1.9	0.000725 ± 0.000036	364 ± 23	69.1 ± 3.4	60 ± 10	146.4 ± 1.9
3881-1256b	Inactive	Spire near Marker H	4018.0 ± 6.9	369.0 ± 6.0	144.9 ± 1.9	0.002495 ± 0.000047	449 ± 11	238.3 ± 4.5	212 ± 27	144.9 ± 1.9
3881-1325	Inactive	Tower from the base of Marker H	3828.9 ± 5.4	16,927 ± 715	145.6 ± 1.7	0.1093 ± 0.0022	408 ± 19	10,923 ± 233	9644 ± 1308	149.6 ± 1.8
H02-072605-R0203	Inactive	From massive carbonate from below M6 vent	2256.4 ± 3.0	5614 ± 165	147.0 ± 1.8	0.0466 ± 0.0013	309 ± 12	4525 ± 128	3806 ± 732	148.5 ± 1.8
H03-072705-R0229	Inactive	From talus slope at base of Poseidon	3391.9 ± 7.1	6140 ± 230	148.1 ± 2.1	0.0377 ± 0.0012	344 ± 17	3645 ± 119	3123 ± 537	149.4 ± 2.1
H03-072705-R0631	Inactive	Talus from the base of Poseidon, below IMAX	4941.1 ± 9.0	1336 ± 29	145.8 ± 2.0	0.00485 ± 0.00018	297 ± 13	464 ± 17	386 ± 80	145.9 ± 2.0
H05-072905-R0238	Inactive	Talus from the base of Poseidon, below IMAX	4415.2 ± 8.7	342.4 ± 6.6	146.6 ± 2.2	0.01126 ± 0.00020	2398 ± 62	1078 ± 19	1055 ± 29	147.0 ± 2.2
H05-072905-R0256	Inactive	Talus from the base of Poseidon, below IMAX	5117.5 ± 7.2	13,797 ± 647	145.4 ± 1.7	0.0730 ± 0.0019	447 ± 24	7,180 ± 188	6,401 ± 805	148.0 ± 1.7
H05-072905-R0347	Inactive	Dark brown deposit from near Razorback	2547.1 ± 4.9	15,199 ± 718	139.7 ± 2.2	0.2140 ± 0.0052	592 ± 31	22,611 ± 609	20,879 ± 1848	148.2 ± 2.4
H07-073005-R2329	Inactive	Massive carbonate east of Poseidon	2213.4 ± 4.1	40,560 ± 4484	113.5 ± 2.5	0.609 ± 0.025	549 ± 65	84,963 ± 5134	79,529 ± 7448	142.1 ± 4.3
H08-080105-R0624	Inactive	From below the Razorback	5483 ± 17	187.3 ± 4.4	146.6 ± 2.9	0.001758 ± 0.000068	850 ± 39	167.6 ± 6.5	158 ± 12	146.7 ± 2.9
H08-080105-R0737	Inactive	Talus from a talus ramp SE of Poseidon	1959.1 ± 5.4	811 ± 19	145.8 ± 3.7	0.03346 ± 0.00063	1334 ± 40	3235 ± 62	3115 ± 135	147.1 ± 3.8

Decay constants are 9.1577×10^{-6} yr^{-1} for ^{230}Th, 2.8263×10^{-6} yr^{-1} for ^{234}U (Cheng et al., 2000b) and 1.55125×10^{-10} yr^{-1} for ^{238}U (Jaffey et al., 1971).

[#] Chimney samples collected using DSV *ALVIN* in 2000 and 2003 are identified by dive number followed by a GMT time stamp (e.g., sample 3881-1338 was collected at 13:38 hours on *ALVIN* Dive #3881). Samples collected in 2005 using the ROV *Hercules* are tagged using the convention dive number-date-sample type-time (e.g., sample H06-073005-R0316 was collected during *Hercules* Dive #6 on July 30, 2005 at 03:16 (GMT) and the "R" denotes rock samples).

[a] $\delta^{234}U = ([^{234}U/^{238}U]_{activity} - 1) \times 1000$.

[b] $[^{230}Th/^{238}U]_{activity} = 1 - e^{\lambda_{230}t} + (\delta^{234}U_{measured}/1000)[\lambda_{230}(\lambda_{230} - \lambda_{234})](1 - e^{-(\lambda_{230}-\lambda_{234})t})$, where t is the age.

[c] The degree of detrital ^{230}Th contamination is indicated by the $[^{230}Th/^{232}Th]$ atomic ratio instead of the activity ratio.

[d] Age corrections were calculated using an average seawater $^{230}Th/^{232}Th$ atomic ratio of $50 \pm 50 \times 10^{-6}$.

[e] $\delta^{234}U_{initial}$ corrected was calculated based on ^{230}Th age (t), i.e., $\delta^{234}U_{initial} = \delta^{234}U_{measured} \times e^{\lambda_{234}t}$, and t is corrected age.

Author's personal copy

crushed and hand-picked to remove biolithic and lithic fragments to minimize contamination from foreign materials such as chips of serpentinite, foraminifera, and shells under a microscope (Ludwig et al., 2006). For two well-lithified chimneys (3871-1512 and 3872-1530), powdered samples were drilled from cut slabs. Subsamples from six chimneys (3651-1022, 3862-1325, H06-073005-R0316, 3871-1512, 3872-1530, and 3881-1338) were analyzed to investigate potential isochron relationships.

4.2. Analytical techniques

4.2.1. *Vent fluids and seawater*

Seawater and hydrothermal fluid samples were prepared in the Minnesota Isotope Laboratory (MIL) at the University of Minnesota using methods described by Chen et al. (1986a) and Shen et al. (2003). All samples were gravimetrically spiked with a synthetic ^{229}Th–^{233}U–^{236}U mixed spike, calibrated with gravimetric U and Th standards (Cheng et al., 2000a,b), to correct for instrumental mass bias and to determine U–Th isotopic and concentration (Chen and Wasserburg, 1981; Chen et al., 1986a). The seawater and vent fluid samples with Mg concentrations >5 mmol/kg were spiked with MIL "Coral-B" spike (8.172 pmol/g ^{233}U and 0.3951 pmol/g ^{229}Th), whereas vent fluids with Mg values <5 mmol/kg were spiked with a diluted (1:20) Speleothem-B spike (0.7327 pmol/g ^{233}U and 0.2116 pmol/g ^{229}Th). Spiked sample was then refluxed in an oven at 60 °C for 7 days to earn a U–Th isotopic equilibrium condition (Moran et al., 2002). After a subsequent co-precipitation step with an iron chloride solution and NH_4OH, U, and Th were separated using anion exchange chromatography methods (Chen et al., 1986a; Edwards, 1988). Dried eluted U and Th aliquots were dissolved in 1% HNO_3 + 0.005 N HF for instrumental analysis.

All samples were analyzed using a Thermo Fisher NEPTUNE multi-collector inductively-coupled plasma magnetic sector mass spectrometer (MC-ICP-MS) in the MIL. Total transmission ionization efficiency in the MC-ICP-MS is 1–2% compared to 0.1–0.2% in the ICP-sector field (SF)-MS (Shen et al., 2002) and 0.1% by TIMS (Edwards et al., 1987). A protocol, using one MasCom secondary electron multiplier (SEM) with repelling potential quadrupole (RPQ), in peak-hopping mode was employed. With the RPQ set to 80–85% transmission, abundance sensitivities were only 0.2–0.3 ppm at 1 atomic mass unit (amu) difference and 0.02–0.04 ppm at 2 amu difference for ^{238}U, and 0.3–0.4 ppm and 0.04–0.06 ppm, respectively, for ^{232}Th. A sample size of only 1–4 ng U is needed to offer the reproducibility (2 RSD) of 1–2‰. No significant difference between measurements of standards, and coral and speleothem samples on ICP-sector-field-MS (ICP-SF-MS) (Shen et al., 2002) and on MC-ICP-MS certify the developed MC-ICP-MS methodology (Cheng et al., 2009; Frohlich et al., 2009). Procedural blanks were subtracted during offline data reduction.

4.2.2. *Chimneys*

Carbonate samples were chemically prepared in the MIL using methods described in Edwards et al. (1986/1987) and Shen et al. (2003). Approximately 0.2 g of carbonate was weighed in acid-cleaned Teflon beakers, dissolved in HNO_3, and then spiked. After adding five drops of $HClO_4$, the samples were capped and heated for 4–6 h to remove organics and equilibrate the spike with the sample. Uranium and Th aliquots were separated using Fe co-precipitation and ion chromatography, dissolved in 1% HNO_3 + 0.005 N HF, and then stored in acid-cleaned plastic ICP-vials. Procedural blanks were measured regularly and three-month average values were 0.02 ± 0.01 pmol ^{238}U, 0.003 ± 0.003 pmol ^{232}Th, and 0.0006 ± 0.0005 fmol ^{230}Th.

All samples were analyzed on an ICP-SF-MS using methods described by Shen et al. (2002). Data reduction was completed off-line as described by Cheng et al. (2000b) and Shen et al. (2002). Uranium and Th isotopic compositions are given in Table 2. Ages were calculated iteratively using Eq. (1). ^{232}Th/^{238}U–^{230}Th/^{238}U–^{234}U/^{238}U isochrons were constructed using *Isoplot 3.00* software (Ludwig and Titterington, 1994; Ludwig, 2003). All measured errors of isotopic and concentration are given as 2 standard deviation of the mean ($2\sigma_m$) and age precisions are reported as 2 standard deviations (2σ) unless otherwise noted.

5. RESULTS

Measured seawater ^{238}U concentrations range from 3.25 to 3.29 ng/g with a mean concentration of 3.28 ± 0.03 ng/g; the mean seawater δ^{234}U is 146.5 ± 0.6 (Table 1). Seawater ^{232}Th concentrations range from 0.13 to 0.14 pg/g with an anomalous high value of 0.443 pg/g for sample H08_080105_M3_0246 (Table 1). Seawater ^{230}Th/^{232}Th atomic ratios vary from 35 $(\pm 7) \times 10^{-6}$ to 48 $(\pm 3) \times 10^{-6}$. The mean seawater ^{230}Th/^{232}Th with its uncertainty is 43 $(\pm 10) \times 10^{-6}$ (Table 1).

In the six fluid samples, Mg concentration varies from 1.1 to 50.0 mmol/kg and ^{238}U concentration ranges from 0.0073 to 3.1 ng/g (Table 1), showing the samples have been mixed with different amounts of ambient seawater during sampling (Ludwig et al., 2006). Only three fluid samples, H04_072805_M1_0416, H06_073005_M4_0413, and 3863m15, have measured Mg concentrations <12 mmol/kg and the ^{232}Th concentration in these samples is 0.11–0.13 pg/g (Table 1). Two fluid samples with 1.1 mmol/kg Mg have ^{230}Th/^{232}Th atomic ratios of 1 $(\pm 10) \times 10^{-6}$ to 11 $(\pm 5) \times 10^{-6}$. Fluids with Mg >12 mmol/kg have ^{232}Th concentrations up to 1.9–2.8 pg/g (Table 1).

Chimney ^{238}U concentrations range from 345 to 10,500 ng/g, and ^{232}Th concentrations range widely from 0.038 to 125 ng/g (Table 2). Measured δ^{234}U values range from 104 to 188 (Table 2). Bulk rock chimney ^{230}Th/^{232}Th atomic ratios span a wide range from 43 $(\pm 8) \times 10^{-6}$ to 530 $(\pm 25) \times 10^{-3}$ (Table 2). All chimney ages are corrected to $^{230}Th_{nr}$ introduced by seawater with an initial ^{230}Th/^{232}Th value of 50 $(\pm 50) \times 10^{-6}$. Corrections for initial $^{230}Th_{nr}$ generally range 5–60% and 0–10% for samples with ages of younger and older than 20 kyrs, respectively (Table 2). Corrected bulk rock chimney ages range from 17 ± 6 yrs to 120 ± 13 kyrs (Table 2). Data from subsamples of the

Author's personal copy

six chimneys analyzed for isochrons are shown in Table 3 and are discussed in Section 6.5.

6. DISCUSSION

6.1. Uranium in seawater and vent fluids

At the LCHF, the in-situ salinity is 35.468 psu at a depth of 745 m, where seawater samples, SW-2, SW-3, SW-4, and SW-5, were collected. The 35.0-psu normalized seawater U concentration of 3.241 ± 0.003 ng/g is undistinguishable from the mean seawater value of 3.238 ng/g (Chen et al., 1986a), indicating the conservative behavior of seawater U at the LCHF. Similarly, the mean measured seawater δ^{234}U of 146.5 ± 0.6 is comparable to the open-ocean values (Robinson et al., 2004; Andersen et al., 2010).

When sampling hydrothermal fluids, the entrainment of some seawater is inevitable. Mg is removed during hydrothermal circulation and its concentration is typically used as an indicator of seawater–fluid mixing (e.g., Butterfield et al., 1994; Mottl and Wheat, 1994). There are three fluid samples (H04_072805_M1_0416, H06_073005_M4_0413, and 3863m15) with low uncorrected Mg concentrations <12 mmol/kg (Table 1). For sample 3863m15, the Mg concentration is 11.3 mmol/kg and the ^{238}U concentration is 0.537 ng/g, suggesting that this sample is mixed with 21% ambient seawater (Table 1 and Fig. 3a). The previous two samples, with 1.1 mmol/kg Mg, can be considered to be much closer to the fluid endmember (98% vent fluid) (Table 1). These samples contain 0.033 and 0.0073 ng/g ^{238}U concentrations and 0.11–0.12 pg/g ^{232}Th, respectively. With an assumption that the endmember fluid Th/U atomic ratio is close to a bulk crustal value of 3.6–3.8 (Taylor and McLennan, 1985, 1995), the endmember fluid U concentration could be only 0.029–0.033 pg/g, indicating that U is scavenged by ultramafic rocks during hydrothermal circulation, similar to observations in oceanic mafic crustal environments (Table 1 and Fig. 3a) (Michard and Albarede, 1985; Chen et al., 1986b). This is supported by results from Boschi et al. (2006), who showed that altered serpentinite basement rocks contain elevated concentrations of U compared to the parent rock.

Chen et al. (1986b) found that vent fluid samples collected from black smokers at the 21°N EPR site had δ^{234}U values ranging from 140 to 200, falling near measured seawater ratios (149 ± 8 to 155 ± 17). Similarly, at the LCHF, the δ^{234}U of the hydrothermal fluids (mean = 144 ± 85) is indistinguishable from that of ambient seawater (mean = 146.5 ± 0.6) (Table 1 and Fig. 4). The similarity of the δ^{234}U ratios between seawater and vent fluids indicates that the input of ^{234}U from α-recoil is not notable (Kigoshi, 1971). Although groundwater studies have shown α-recoil to be a potentially significant input of U-series daughter isotopes to aquifer solutions in reducing environments (Voltaggio et al., 1998), this process does not appear to have an effect on ^{234}U and ^{230}Th values in the Lost City fluids. The δ^{234}U values of the two fluid samples with the lowest Mg concentration are 92 ± 116 and 154 ± 31 and the poor analytical precision is caused by their extremely low ^{238}U concentrations (only 0.7 ng and 6.7 ng, respectively). These values provide a first-order estimate of the U isotopic composition of the LCHF vent fluids.

6.2. Thorium in seawater and vent fluids

Except for seawater sample H08_080105_M3_0246, ambient seawater proximal to the LCHF has a mean ^{232}Th concentration of 0.133 ± 0.016 pg/g, which is within error of previously measured Atlantic seawater at 800 m (Moran et al., 1997, 2002). The high ^{232}Th concentration of 0.443 ± 0.013 pg/g in sample H08_080105_M3_0246 is likely due to the entrainment of some detritus from the top of the carbonate cap, where it was collected.

By comparison, the ^{232}Th concentration in hydrothermal fluids is variable. Chen et al. (1986b) noted that fluids egressing from black smokers at the EPR had variable ^{232}Th concentrations ranging from 1 to 4.3 pg/g, which were much higher than ambient seawater (<0.17 pg/g), and concluded that Th may be leached from the crust during water–rock interaction at depth. Similarly, LCHF vent fluids have variable ^{232}Th concentrations (Table 1 and Fig. 5). The three fluid samples, H04_072805_M1_0416, H06_073005_M4_0413, and 3863m15, with 1.1–11 mmol/kg Mg have ^{232}Th concentrations of 0.11–0.13 pg/g and are within error the same as ambient seawater (Table 1 and Fig. 3b). However, three fluid samples, H02_072605_M1_0443, H03 072705_M3_0354, and H07_073105_M2_1238, have anonymously high ^{232}Th concentrations compared to seawater, ranging from 1.86 to 2.20 pg/g (Table 1 and Fig. 3b). This observation cannot be explained by vent location: samples collected from the same vent structures (e.g., Marker 3 and Marker H) on different days have much lower ^{232}Th concentrations (Table 1). In 2005, we cleaned each major sampler with 1.5 N HNO_3; however, even after adding this step to the cleaning process, there is no noticeable difference in ^{232}Th concentration or ^{230}Th/^{232}Th ratios (Table 1).

Fig. 5 shows that sample 3863m15 is a mix of fluid and ambient seawater. However, three samples with high-^{232}Th do not lie in the mixing zone on the plot (Fig. 5). Trivial amounts of chimney carbonate detritus with high ^{232}Th and ^{230}Th/^{232}Th could likely be collected in these samples. Contamination from particulate matter during collection on board could also be possible. More measurements of large fluid sample volumes would be required to better evaluate these high values and to evaluate endmember fluid Th concentrations.

The vent fluids at the LCHF have lower ^{230}Th/^{232}Th atomic ratios ($1–11 \times 10^{-6}$) than seawater ($35–48 \times 10^{-6}$) (Table 1 and Fig. 3c). This trend holds when the ^{230}Th/^{232}Th atomic ratios are plotted against 1/[^{232}Th] (Fig. 5). The low ^{230}Th/^{232}Th atomic ratios of the fluids are attributed to the low concentrations of the parent isotopes (^{238}U and ^{234}U) in the fluids. The low ratios also indicate that α-recoil does not contribute additional ^{230}Th to the fluids.

6.3. U and Th systematics in LCHF chimneys

Uranium in the endmember LCHF fluids is likely <0.0073 ng/g, which is significantly lower than 3.28 ng/g

Author's personal copy

Table 3
U–Th data from subsamples of LCHF chimneys used for isochrons.

Sample ID	Sample type	^{238}U (ng/g)	^{232}Th (pg/g)	$\delta^{234}U_{measured}$ [a]	$[^{230}Th/^{238}Th]$ activity [b]	$[^{230}Th/^{232}Th]$ (ppm) [c]	Age (years) uncorrected
3651-1022	Active	2820.0 ± 5.4	884.4 ± 2.7	149.2 ± 1.6	0.001406 ± 0.000025	74.0 ± 1.3	133.7 ± 2.4
3651-1022		2007.9 ± 2.4	81.7 ± 3.7	146.1 ± 1.6	0.000592 ± 0.000099	240 ± 42	56.4 ± 9.4
3651-1022		2822.8 ± 3.7	137.9 ± 4.7	144.7 ± 1.7	0.000672 ± 0.000082	227 ± 29	64.1 ± 7.8
3651-1022		2762.1 ± 3.4	126.1 ± 4.2	145.1 ± 1.8	0.000670 ± 0.000046	242 ± 19	63.9 ± 4.4
3651-1022a		3411.7 ± 5.9	57.0 ± 3.6	144.0 ± 2.0	0.000285 ± 0.000023	282 ± 29	27.2 ± 2.2
3651-1022b		3028.0 ± 4.9	128.4 ± 4.3	142.1 ± 1.9	0.000754 ± 0.000038	294 ± 18	72.1 ± 3.7
3651-1022c		3214.5 ± 5.2	82.2 ± 4.2	143.6 ± 1.9	0.000489 ± 0.000031	315 ± 26	46.7 ± 2.9
3862-1325	Active	2356.3 ± 3.3	468 ± 26	148.0 ± 1.8	0.000939 ± 0.000046	78.1 ± 5.7	89.4 ± 4.4
3862-1325a		3098.4 ± 4.3	77.5 ± 3.2	141.5 ± 1.6	0.000253 ± 0.000021	167 ± 15	24.2 ± 2.0
3862-1325b		2542.7 ± 3.5	73.5 ± 3.6	145.6 ± 1.7	0.000456 ± 0.000036	260 ± 24	43.4 ± 3.5
3862-1325c		4229.0 ± 6.5	121.3 ± 4.6	140.7 ± 1.7	0.000459 ± 0.000022	264 ± 16	43.9 ± 2.1
3862-1325d		4134.8 ± 6.2	84.3 ± 3.5	140.6 ± 1.6	0.000284 ± 0.000020	230 ± 19	27.2 ± 1.9
3862-1325e		3646.8 ± 5.3	73.3 ± 4.3	142.8 ± 1.7	0.000343 ± 0.000027	282 ± 28	32.8 ± 2.6
H06-073005-R0316_1	Active	3280.2 ± 4.6	82.6 ± 3.9	146.1 ± 1.9	0.000523 ± 0.000033	343 ± 27	49.9 ± 3.2
H06-073005-R0316_2		2836.3 ± 4.4	68.7 ± 3.1	143.7 ± 1.8	0.000499 ± 0.000036	340 ± 29	47.7 ± 3.4
H06-073005-R0316_3		3263.7 ± 8.4	81.3 ± 3.8	145.5 ± 3.2	0.000541 ± 0.000042	358 ± 32	51.5 ± 4.0
H06-073005-R0316_4		3480.6 ± 4.2	72.6 ± 3.6	144.1 ± 1.5	0.000441 ± 0.000034	350 ± 32	42.1 ± 3.2
H06-073005-R0316_5		3004.8 ± 4.7	71.9 ± 3.5	144.6 ± 1.8	0.000510 ± 0.000040	352 ± 32	48.6 ± 3.8
3871-1512	Inactive	3673.6 ± 4.1	46471 ± 250	144.3 ± 1.7	0.1894 ± 0.0017	247.2 ± 2.6	19,683 ± 198
3871-1512A		3866.8 ± 6.1	150 ± 4.3	140.9 ± 1.8	0.04925 ± 0.00024	20979 ± 605	4815 ± 25
3871-1512B		3888.8 ± 6.5	1014 ± 16	147.0 ± 2.0	0.06198 ± 0.00043	3925 ± 69	6060 ± 45
3871-1512C		4471 ± 152	6498 ± 191	173 ± 59	0.0682 ± 0.0027	774 ± 27	6531 ± 433
3871-1512D		3447.3 ± 4.3	129.7 ± 3.8	145.4 ± 1.7	0.000434 ± 0.000037	191 ± 17	41 ± 3.5
3872-1530	Inactive	4801.8 ± 6.1	1204 ± 19	105.2 ± 1.7	0.3599 ± 0.0019	23,693 ± 395	42,734 ± 285
3872-1530a		2450.9 ± 3.8	18.8 ± 7.1	237.8 ± 2.1	0.3711 ± 0.0023	799,087 ± 300,808	38,442 ± 291
3872-1530b		3794.0 ± 6.0	34.1 ± 4.2	142.8 ± 1.9	0.3593 ± 0.0030	660,496 ± 81,375	40,878 ± 415
3872-1530c		3859.3 ± 6.2	43.5 ± 3.4	146.8 ± 1.9	0.3902 ± 0.0026	571,231 ± 45,185	44,971 ± 385
3872-1530d		4204.7 ± 6.7	21.1 ± 4.1	116.6 ± 1.9	0.3566 ± 0.0041	1,171,925 ± 225,679	41,702 ± 588
3872-1530e		3318.1 ± 4.8	10.9 ± 3.2	187.4 ± 1.9	0.3595 ± 0.0025	1,799,775 ± 519,472	38,976 ± 325
3881-1338/3 (Interior)	Inactive	1549.0 ± 1.9	177 ± 20	149.0 ± 1.6	0.00729 ± 0.00011	1056 ± 122	695 ± 10
3881-1338/4 (Interior)		2018.9 ± 2.1	235 ± 18	148.1 ± 1.3	0.00734 ± 0.00012	1041 ± 81	700 ± 11
3881-1338/5 (Interior)		2352.3 ± 2.7	229 ± 17	147.0 ± 1.5	0.007056 ± 0.000066	1198 ± 87	673.7 ± 6.3
3881-1338/6 (Interior)		2.845.8 ± 2.8	353 ± 22	145.5 ± 1.5	0.007231 ± 0.000076	961 ± 61	691.4 ± 7.4
3881-1338/7 (Interior)		2.372.0 ± 2.1	390 ± 23	145.6 ± 1.4	0.007650 ± 0.000084	768 ± 47	731.5 ± 8.1
3881-1338/A (Exterior)		2.380.6 ± 2.8	17,470 ± 82	145.5 ± 1.8	0.07268 ± 0.00078	163.5 ± 1.9	7.149 ± 80
3881-1338/B (Exterior)		2.050.7 ± 2.4	10,039 ± 45	145.2 ± 1.7	0.05038 ± 0.00053	169.9 ± 1.9	4.909 ± 53
3881-1338/C (Exterior)		2.544.5 ± 2.8	18,954 ± 110	147.0 ± 1.6	0.07105 ± 0.00088	157.5 ± 2.2	6.973 ± 90
3881-1338/D (Exterior)		1.921.8 ± 2.0	13,724 ± 59	147.4 ± 1.6	0.07239 ± 0.00069	167.4 ± 1.7	7.106 ± 71
3881-1338/E (Exterior)		4.051.5 ± 5.2	14,559 ± 62	148.0 ± 1.7	0.03823 ± 0.00037	175.6 ± 1.8	3.696 ± 36

[a] $\delta^{234}U = ([^{234}U/^{238}U_{activity} - 1) \times 1000$.
[b] $[^{230}Th/^{238}U]_{activity} = 1 - e^{\lambda_{234}t} + (\delta^{234}U_{measured}/1000)[\lambda_{230}/(\lambda_{230} - \lambda_{234})](e^{(\lambda_{234}-\lambda_{234})t})$, where t is the age.
[c] The degree of detrital ^{230}Th contamination is indicated by the $[^{230}Th/^{232}Th]$ atomic ratio instead of the activity ratio.

U in the ambient seawater. An average value for $\delta^{234}U_{initial}$ data with precision better than 3.0‰ in chimney carbonates is 147.2 ± 0.8 (Table 2), matching the seawater value of 146.5 ± 0.6 (Table 1). In an assumptive mixing model, using an arbitrarily low vent fluid $\delta^{234}U$ of 100 and the water mixture with 90% fluid and 10% seawater, the $\delta^{234}U$ of the precipitate would be 145.6, still very close to the seawater value. The results indicate that U in the chimneys is seawater-derived. U concentrations in the LCHF carbonates vary from <1 to 10 μg/g; they are not a function of chimney age or type (Table 2 and Fig. 6a). Even within the same structure, U concentration can vary by >600 ng/g, which is outside of analytical error (e.g., samples 3651-1022, H06-073005-R031, and 3881-1338), showing the heterogeneity of the chimney ^{238}U concentration (Table 3).

^{232}Th concentrations vary widely across the field and individual chimneys contain variable amounts of Th. In general, the inactive chimneys contain a wider range of ^{232}Th (0.084–125 ng/g) and higher average ^{232}Th concentration (26.1 ng/g) than active chimneys (which range from 0.038 to 8.95 ng/g with a mean ^{232}Th concentration of 0.81 ng/g). Thorium concentration generally increases with chimney age (Fig. 6c), which is likely due to detrital accumulation, Th scavenging from ambient seawater, and the formation of manganese crust over time (Ludwig et al., 2006).

Author's personal copy

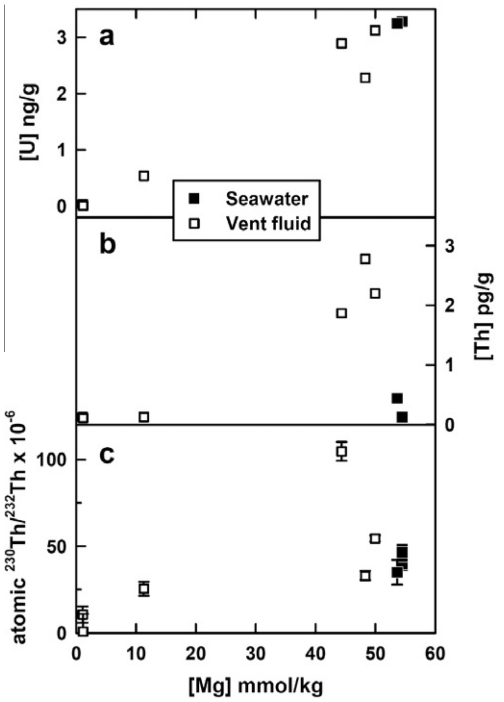

Fig. 3. Seawater (solid squares) and vent fluid (hollow squares) chemistry. (a) LCHF fluid end-members have near-zero U and Mg concentrations, showing these elements are removed from seawater during hydrothermal circulation through the Atlantis Massif. (b) Thorium concentrations in the LCHF fluids are variable compared to surrounding seawater. Fluid samples with <12 mmol/kg Mg have ^{232}Th concentrations similar to seawater while three fluid samples have significantly higher ^{232}Th. This difference is not explained by vent location and is attributed to possible contamination by particulate matter. (c) Near end-member fluids (containing 1.1 mmol/kg Mg) have low ^{230}Th/^{232}Th atomic ratios compared to surrounding seawater. The vent fluids do not represent an additional source of initial ^{230}Th to the carbonates. The error bars are smaller than the symbol size for almost all samples.

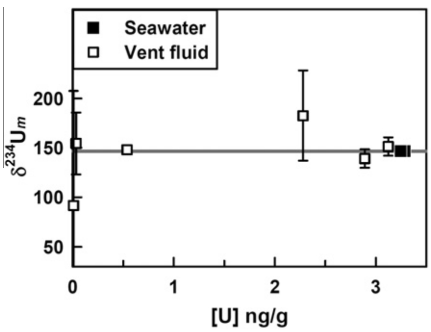

Fig. 4. A plot of $\delta^{234}U_m$ vs. [U] for seawater (solid squares) and vent fluid (hollow squares) samples. The δ^{234}U values of the LCHF fluids are not distinguishable from the δ^{234}U range of ambient seawater (146.5 ± 0.6; gray line).

6.4. Sources of initial ^{230}Th

In any system, the addition of $^{230}Th_{nr}$ can make a sample appear *falsely old*. At the LCHF, there are three

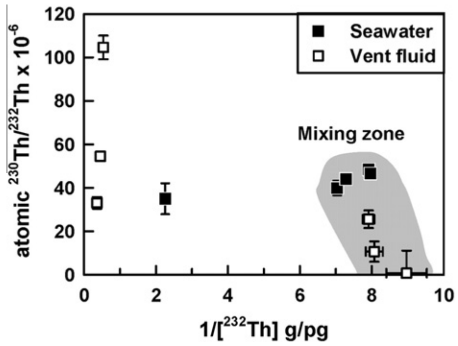

Fig. 5. A plot of ^{230}Th/^{232}Th atomic ratio vs. 1/^{232}Th for LCHF seawater (solid squares) and fluid (hollow squares). The concentration of ^{232}Th and the ^{230}Th/^{232}Th ratio in both seawater and vent fluids collected from the LCHF are variable. These differences are attributed to the non-conservative and particle reactive behavior of Th in the ocean. Gray area denotes the mixing zone of only fluid and ambient seawater.

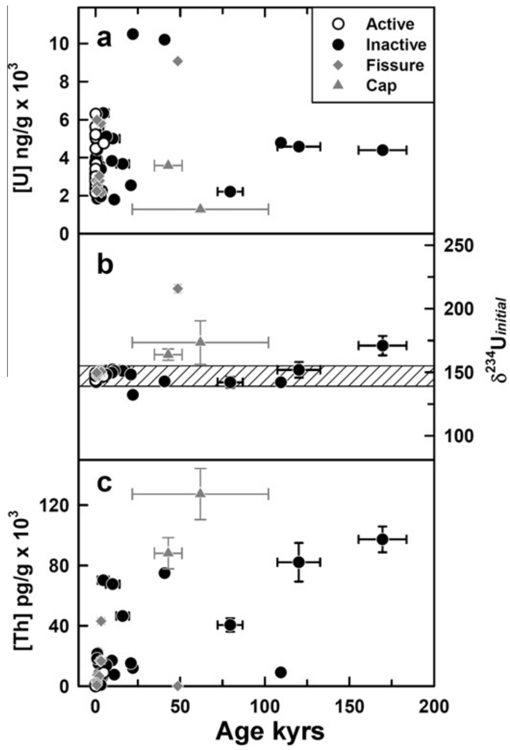

Fig. 6. Temporal chimney U–Th chemistry. (a) The concentration of U in the LCHF chimneys varies from 1 to 10 × 10^3 ng/g and there is no correlation between chimney age or chimney type and U concentration. (b) The $\delta^{234}U_{initial}$ of most LCHF carbonate chimneys is near the ambient seawater value of 146.5 ± 0.6. Chimneys with $\delta^{234}U_{initial}$ outside the 139–155 criterion (shaded) have likely experienced diagenesis. (c) The LCHF chimneys are heterogeneous with respect to ^{232}Th concentration. In general, chimney ^{232}Th increases with age due to the accumulation of detritus and formation of Mn-crust on the exterior of the chimneys. Carbonate cap samples have some of the highest ^{232}Th concentrations, most likely due to the significant amount of detrital material that is cemented into the cap rock. In most cases the error bars are smaller than the symbol size.

Author's personal copy

potential "external" sources of $^{230}Th_{nr}$: seawater, hydrothermal fluid, and detritus. The LCHF chimneys are also likely subject to input of $^{230}Th_{nr}$ by "internal" processes that may include α-recoil and diagenesis. Because of the unique geochemical setting of the LCHF carbonates and the importance of quantifying $^{230}Th_{nr}$ for age dating, each source of $^{230}Th_{nr}$ is addressed and quantified in the following discussion.

6.4.1. Seawater

In seawater, Th is insoluble and easily sorbs onto particles: it generally has very low solubility except in alkaline conditions (e.g., Bacon and Anderson, 1982). Because of its particle-affinity, Th is rapidly removed from the water column with marine detritus. Consequently, Th has a short average residence time in the sea of only ~20 yrs (e.g., Dunk et al., 2002; Cochran and Masqué, 2003; Henderson and Anderson, 2003). Seawater ^{230}Th concentration and $^{230}Th/^{232}Th$ increase with depth and seawater can be a significant source of $^{230}Th_{nr}$ to deep sea carbonates including deep sea corals and the LCHF chimneys (e.g., Bacon and Anderson, 1982; Cheng et al., 2000a; Edwards et al., 2003).

6.4.2. Vent fluid

The actively venting chimneys at the LCHF have $^{230}Th/^{232}Th$ atomic ratios that are significantly higher than that of seawater (74–483 × 10^{-6}) (Table 2). However, the $^{230}Th/^{232}Th$ atomic ratio of vent fluids (1–11 × 10^{-6}) at the LCHF is relatively low in comparison to seawater (Table 1). Assuming that the $^{230}Th/^{232}Th$ ratio of the fluids is relatively constant over time, these results show seawater will contribute more Th to carbonate deposits than will vent fluids. The high $^{230}Th/^{232}Th$ ratios in the active chimneys may be attributed to "whiffs" of ^{230}Th from nearby older carbonate.

6.4.3. Detritus

Within the LCHF, detritus can come in many forms, including marine snow, marine sediments, and talus and/or fragments of old carbonate deposits. Detrital input of Th to the chimneys is difficult to quantify without an extensive study of sediment trap and filtered seawater samples. However, to a first order, the measured concentration of ^{232}Th in the carbonates can be used as an indicator of detrital ^{230}Th. In general, the inactive chimneys have high concentrations of ^{232}Th (Fig. 6c) showing that detrital material may be contributing Th to the structures. This is observed in some of the chimney hand samples which incorporate biolithic and lithic fragments in their outer walls (Ludwig et al., 2006). The $^{230}Th/^{232}Th$ atomic ratios of the inactive chimneys range widely, from 84 to 4000 × 10^{-6} (Table 2 and Fig. 7). Carbonate talus collected from the base of Poseidon has ^{232}Th concentrations of up to 0.3–14 ng/g, which shows that some of these samples may have incorporated substantial detrital ^{230}Th (Table 2). In contrast, the ^{232}Th concentrations of the active chimneys are lower, and the $^{230}Th/^{232}Th$ atomic ratios fall in a smaller range of 74–83 × 10^{-6} (Table 2 and Fig. 7). This trend indicates that most of the active chimneys do not incorporate much detrital ^{230}Th. Samples from the carbonate cap, which is composed of hydrothermally-cemented sediments, have the highest ^{232}Th concentrations at 127 ± 17 ng/g, attributed to detrital accumulation. However, the $^{230}Th/^{232}Th$ ratios of the cap samples vary from 43 to 86 × 10^{-6}, showing that they have likely experienced diagenesis (see Section 6.5.2). Quantifying the contribution of detrital ^{232}Th to the chimneys is complicated as evidenced by an absence of a consistent trend between chimney age and ^{232}Th (Fig. 6c) and the highly variable ^{232}Th concentrations throughout the field regardless of chimney type.

6.4.4. α-Recoil

α-Recoil is a significant source of $^{230}Th_{nr}$ for marine sediments and in some marine carbonates in near-surface environments (e.g., Cochran and Masqué, 2003; Thompson et al., 2003; Robinson et al., 2004). In the LCHF chimneys, which are at intermediate-water depth with high seawater $^{230}Th/^{232}Th$ atomic ratios [35 (±7) × 10^{-6} to 48 (±3) × 10^{-6}], the impact of α-recoil is assumed to be minimal compared to the other inputs described above.

Conclusively, seawater and detritus are the most important factors to consider when assessing the $^{230}Th_{nr}$ corrections for the LCHF chimney ages. Given these sources, the range of possible initial $^{230}Th/^{232}Th$ is 35 × 10^{-6} to >500,000 × 10^{-6}, where most of the high values are found in older samples with high concentrations of radiogenic ^{230}Th.

6.5. Isochrons and ^{230}Th age corrections

To assess the most appropriate $^{230}Th/^{232}Th$ value to use for $^{230}Th_{nr}$ corrections, we explored the conventional tool of isochrons (e.g., Ludwig and Titterington, 1994; Dorale et al., 2001; Edwards et al., 2003; Ludwig, 2003; Shen et al., 2008). Unlike well-banded corals, the LCHF

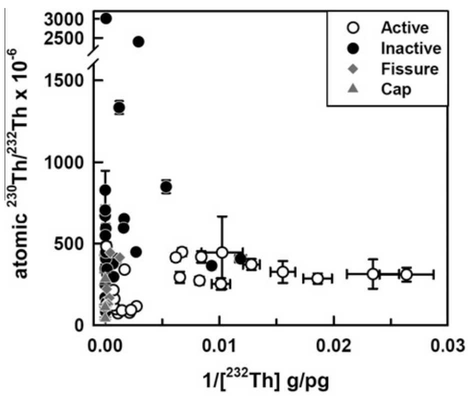

Fig. 7. A plot of $^{230}Th/^{232}Th$ vs. $1/^{232}Th$ in LCHF chimneys. The inactive structures have a wider range of $^{230}Th/^{232}Th$ atomic ratios than their actively venting counterparts. This is likely due to the age of the sample (hence high ^{230}Th) and/or the increased amount of detritus within the structure. Despite variable ^{232}Th concentrations, the active structures have relatively low $^{230}Th/^{232}Th$ atomic ratios. Note that samples 3872-1530 and H03-072605-R2252 with respective high $^{230}Th/^{232}Th$ atomic ratios of 6.1 × 10^{-3} and 5.3 × 10^{-1} are not shown (see Table 2).

Author's personal copy

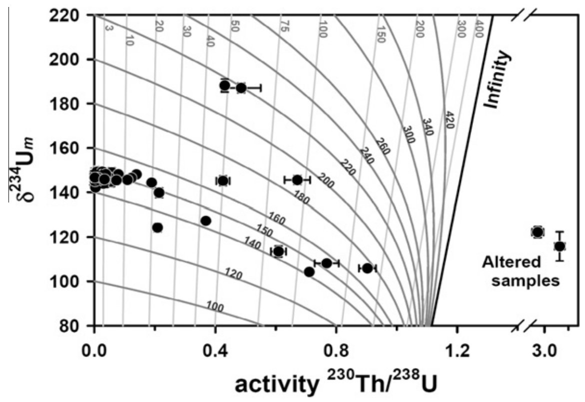

Fig. 8. A plot of measured δ^{234}U vs. ^{230}Th/^{238}U activity ratio. Light gray lines are lines of constant age, given with numbers in kyrs next to the lines. Dark gray contours are lines of constant $\delta^{234}U_{initial}$. Most of the LCHF carbonate samples (circles) fall near seawater δ^{234}U. Two inactive chimneys, 3873-1233 and 3877-1501, fall to the right of infinite age and their age cannot be determined using closed-system age equations.

chimneys are heterogeneous and completely lack banding or obvious growth horizons (Fig. EA-2). Hand samples of the actively venting deposits are fragile, with up to 50% porosity and have sinuous interior micro-channels that make subsampling difficult (Fig. EA-2a and b, Ludwig et al., 2006). In contrast, hand samples of numerous inactive chimneys are massive and require drilling to collect interior subsamples (Fig. EA-2c and d). Subsamples from three active chimneys (samples 3651-1022, 3862-1325, and H06-073005-R0316) and three inactive structures (samples 3871-1512, 3872-1530, and 3881-1338) were collected in an attempt to use isochrons to evaluate the initial ^{230}Th in the LCHF chimneys.

6.5.1. Isochrons and initial ^{230}Th/^{232}Th estimate

Plots of six ^{230}Th/^{238}U vs. ^{232}Th/^{238}U of ^{232}Th/^{238}U–^{230}Th/^{238}U–^{234}U/^{238}U isochrons are shown in Fig. 9. The lack of linearity underscores the chemical heterogeneity of the chimneys, which is also demonstrated by variable ^{238}U and ^{232}Th concentrations and variable ^{230}Th/^{232}Th ratios (Table 3). An isochron for sample 3881-1338 displays the best linear correlation (Fig. 9f), despite chemical heterogeneity (Table 3). Chimney sample 3881-1338 is one of the few large (97.5 cm in length) structures that was recovered in its entirety and provides a unique opportunity to compare the geochemical composition of subsamples from the interior and exterior of the structure (Fig. EA-2e and f). Although the chimney was not visibly venting, geochemical analyses of trace metals indicated that the chimney had a strong vent fluid signal in its interior (Ludwig et al., 2006). In our U–Th analyses, there is a distinct difference in the ^{232}Th concentrations from the interior (0.18–0.40 ng/g) to the exterior (10–19 ng/g) and these values correlate to high ^{230}Th/^{232}Th ratios in the interior and low ^{230}Th/^{232}Th ratios in the exterior, respectively (Table 3). Collectively, subsamples from the interior and exterior of this chimney demonstrate the best isochron relationship found in this study (Fig. EA-2f).

Examining the $\delta^{234}U_{initial}$ value of the chimney samples is also instructive for evaluating the initial ^{230}Th/^{232}Th of the system. Most corrected $\delta^{234}U_{initial}$ data reflect the seawater value. The anomalous corrected $\delta^{234}U_{initial}$ for the inactive sample 3872-1530 (Table 3) suggests that this sample has most likely been altered. Except for this sample, the other five isochron-determined initial ^{230}Th/^{232}Th ratios range from near-vent fluid values (e.g., 10.3 ($\pm$2.1) $\times 10^{-6}$ for active sample 3651-1022) to near seawater values (64 ($\pm$36) $\times 10^{-6}$ for active sample H06-073005-R0316) (Table 3). Considering the Th isotopic compositions in the two sources, seawater and vent fluid, and the $^{230}Th_{nr}$ variability for the five isochrons with the seawater-value $\delta^{234}U_{initial}$, the initial ^{230}Th/^{232}Th ratio is estimated to be 50 ($\pm$50) $\times 10^{-6}$. This value is used to calculate the formation age of the chimney carbonate.

6.5.2. Diagenesis and criteria for fidelity of ^{230}Th Age

In any carbonate system, diagenesis can shift U–Th ratios, indicating open system behavior (e.g., Hamelin et al., 1991; Gallup et al., 1994; Cutler et al., 2003; Stirling and Andersen, 2009). At the LCHF, some of the old samples show physical signs of alteration: some have been recrystallized and resemble marble, while others have micritic calcite filling former pore spaces (Fig. EA-2c and d) (Früh-Green et al., 2003; Ludwig et al., 2006). Geochemical analyses can be used to confirm these physical signs of diagenesis, and the $\delta^{234}U_{initial}$ of these samples can be used as an indicator of open system behavior (e.g., Edwards et al., 1986/1987; Cheng et al., 2000a; Cutler et al., 2003; Robinson et al., 2004; Stirling and Andersen, 2009).

Similar considerations have been used in studies examining the U–Th systematics of corals (e.g., Gallup et al., 1994; Cheng et al., 2000a). Cutler et al. (2003) and Stirling and Andersen (2009) established a U isotopic composition criterion to assess coral samples for alteration. Samples with $\delta^{234}U_{initial}$ within $\pm 8‰$ of the modern marine value and with a 2σ error $\leqslant 8‰$ in the δ^{234}U value can be considered to experience minimal alteration. The same δ^{234}U criterion was applied to the LCHF chimneys as an indicator of diagenesis.

The LCHF carbonate ages span two glacial–interglacial cycles. Previous studies have shown that the δ^{234}U of the ocean has been relatively constant during the last 400 kyrs averaged over glacial and interglacial cycles (Gallup et al., 1994; Henderson and Anderson, 2003). Accordingly, changes in the LCHF carbonate δ^{234}U can be reasonably attributed to diagenesis. The seawater δ^{234}U at the LCHF is 146.5 ± 0.6, so LCHF chimney samples that have $\delta^{234}U_{initial}$ values ranging from 139 to 155 are considered unaltered: this criterion range is shaded in Fig. 6b. The altered samples (which account for 14% of total samples) are typically the older structures which have δ^{234}U values that are significantly higher or lower than seawater δ^{234}U value. Samples 3651-0938a and H03-072605-R2252, for example, have $\delta^{234}U_{initial}$ values 132.2 ± 2.0 and 215.8 ± 3.3, respectively (Table 2 and Fig. 6b). Both cap rock samples have high ^{232}Th concentrations (88 ± 10 to 127 ± 17 ng/g) and $\delta^{234}U_{initial}$ values (163.8 ± 4.4 and 173.4 ± 17.1) that deviate significantly from that of seawater (Table 2 and

Author's personal copy

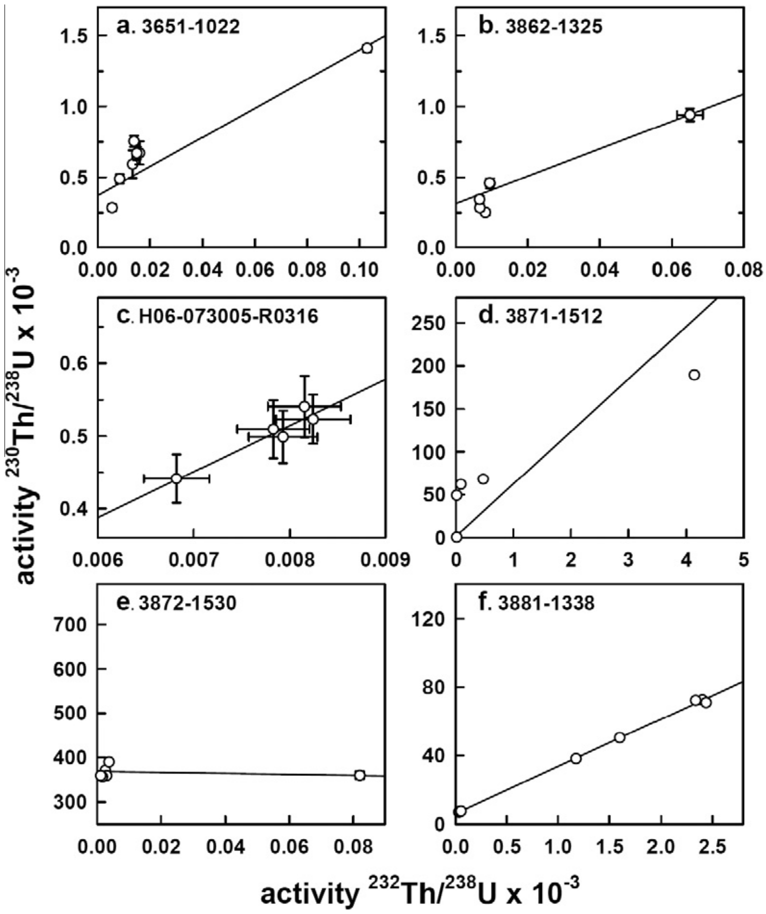

Fig. 9. Isochron plots of $^{230}Th/^{238}U$ vs. $^{232}Th/^{238}U$. Subsamples from three active (a–c) and three inactive (d–f) chimney samples were selected for isochrons to better assess the initial $^{230}Th/^{232}Th$ ratio in the LCHF chimneys.

Fig. 6b). However, it is likely that the cap rock has experienced significant diagenesis and therefore these ages require further evaluation. The oldest chimney with a $\delta^{234}U$ within the defined $\delta^{234}U$-alteration criterion is sample number 3872-1544b which is 120 ± 13 kyrs old. Most of the LCHF carbonate samples fall near the $\delta^{234}U = 150$ in the plot of measured $\delta^{234}U$ vs. $^{230}Th/^{238}U$ activity ratio (Fig. 8). This is consistent with marine carbonates that are believed to have maintained a closed-system (e.g., Edwards, 1998, Cheng et al., 2000b; Cutler et al., 2003). For the samples falling to the right of the "infinite" age contour and experiencing diagenesis [e.g., samples 3873-1233, and 3877-1501 (Table 2 and Fig. 8)], open-system models would potentially give constrained U–Th age (e.g., Villemant and Feuillet, 2003; Thompson et al., 2003).

6.6. Constraints on chimney growth rate and age

For the LCHF, the only constraints that can be currently placed on chimney growth rates come from examination of the "Beehive" structure, which is a fragile chimney growing on the north side of Poseidon that emits the hottest (91 °C) fluids measured in the field (Kelley et al., 2005). During the 2003 expedition, the 30 cm-tall Beehive chimney was sampled (3876-1436) and subsequently the entire chimney fell apart. In 2005, a ~1 m-tall "new Beehive" chimney had re-grown from the same orifice and the structure was sampled again (H06-073005-R0316). Images of the Beehive structures in 2003 and 2005 are shown in Electronic annex Figure EA-3. The Beehive samples provide a constraint on chimney growth rate of 50 cm/yr. By comparison, the rim of the IMAX flange had re-grown by only 25 cm following sampling by *ALVIN* in 2003 and other chimneys that were toppled during the 2003 expedition had not re-grown when we returned to the same sites in 2005 (Kelley et al., 2005). Therefore, 50 cm/yr is believed to be a *maximum* growth rate.

Similar to most of the actively venting structures at the LCHF, the measured $^{230}Th/^{232}Th$ atomic ratio of the Beehive chimney (sample H06-073005-R0316) is anonymously high ($253–372 \times 10^{-6}$) compared to the seawater value (Table 2). Although sample H06-073005-R0316 is only 2 yrs old, when using Eq. (1) and correcting the data to $^{230}Th_{nr}$ introduced by seawater, the age of this structure is 34 ± 10 to 46 ± 8 yrs old (Table 2). The apparent discrepancy between the calculated and true dates suggests that the high-$^{230}Th/^{232}Th$ detritus carbonate from the broken orifice may have been incorporated into the growing matrix. It is

Author's personal copy

important to recognize that the chimney ages presented in Table 2 represent bulk rock ages: these values are a first-order estimation of chimney age. In order to further quantify the development of individual chimneys and the U–Th systematics of Lost City, further analyses such as millimeter- to centimeter-scale subsampling and/or laser ablation ICP-MS (e.g., Potter et al., 2005; Eggins et al., 2008) would be needed.

6.7. Distribution of chimney ages

Results from this investigation provide the first comprehensive analysis of the age distribution of chimneys and carbonate talus in the LCHF (Fig. 10). The youngest deposits in the field are the actively venting structures, which range in ^{230}Th age from 17 yrs (3864-1537) to 4.8 kyrs (H07-073105-R1053) (Table 2). These characteristically fragile, aragonite and brucite-dominated formations are found at the *top* of massive chimneys such as Poseidon and the Nature Tower (Marker H) and also as parasitic growths on the *sides* of large structures (e.g., the Beehive chimney and IMAX flange) (Fig. 10). These young deposits emit the hottest temperature (up to 91 °C at Beehive and 55 °C at IMAX) and the highest pH fluids (up to 11 at IMAX), with the lowest Mg concentrations (0.91 mmol/kg at Beehive) (Kelley et al., 2005). The oldest samples (up to 120 ± 13 kyrs) come from the SSW portion of the field. Several of these samples are from talus deposits that are commonly found at the base of numerous large structures: the moderate to steep exposure on the southern side of the field creates a catch-basin for this debris.

Most samples of measured LCHF carbonate chimneys are less than 5 kyrs old (Table 2). However, geologic sampling using the DSV *ALVIN* or ROV *Hercules* is biased towards collecting rocks that are easily broken off or picked up from talus ramparts. Because the chimneys become harder and more lithified with age, fewer older samples have been collected and analyzed. Despite the bias in sampling, results from this study show that the loci of venting has become more focused over time and that the structures are highly complex. In the following discussion, we present a model for the tectonic and hydrothermal evolution of the field based on spatial relationships and ages of the chimneys, fissures, talus, and cap rock.

7. THE DEVELOPMENT OF THE LCHF AND IMPLICATIONS FOR LONG-LIVED VENTING

Our current model envisions that the central Poseidon complex is supported by an underlying, "stable" plumbing system that has supplied fluids for several thousands of years to this site (Figs. 10 and 11). Because the Poseidon complex has the highest temperature and pH fluids, there is likely a central, insulated set of conduits that focus fluid flow from depth (Fig. 11). This interpretation is consistent with hydrogen isotopic measurements by Proskurowski et al. (2006), which show that fluid temperatures in the warmest vents are similar to those predicted by geothermometric values from $\delta D\text{-}CH_4$ and $\delta D\text{-}H_2$ analyses.

The array of carbonate deposits west and east of Poseidon lies along a well-defined lineament that is interpreted to represent the trace of a W–E striking fault (Fault "A" in Figs. 1 and 10) (Kelley et al., 2005; Karson et al., 2006). The oldest samples recovered are generally near the edges of the Poseidon complex and may represent the underlying foundation of the LCHF, which has been overgrown by the massive Poseidon edifice. These observations indicate that the fault-conduit system that feeds the W–E array of chimneys and the Poseidon complex is exceedingly long-lived and that venting and resultant carbonate deposition created the foundation for larger, massive structures such as Poseidon.

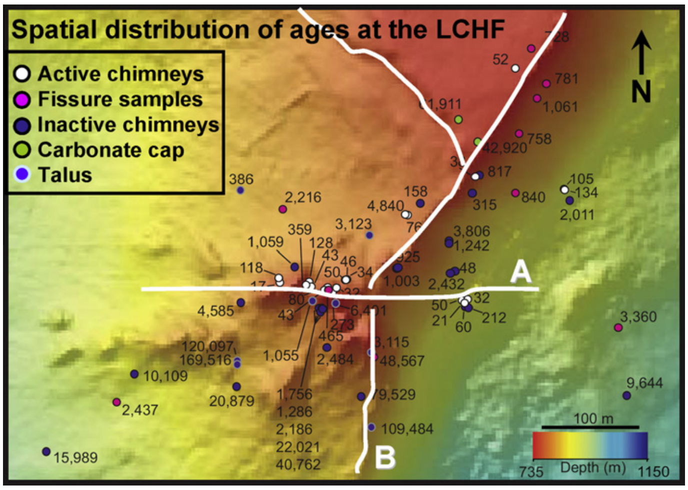

Fig. 10. Spatial relationship of chimney ages in the LCHF. Ages are shown in years. Ages of samples collected during DSV *ALVIN* Dive # 3880 are not included on the map due to navigation problems during the dive. All samples were collected in situ unless marked as talus. The youngest chimneys are located in the Poseidon complex, in some active carbonate deposits that cut the summit cap rock, and along the steep East Wall where seeps are common. The oldest samples are located in the southwestern portion of the field along a near-linear array of W–E trending carbonate deposits. This trend is interpreted to represent the surface expression of an underlying fault system.

Author's personal copy

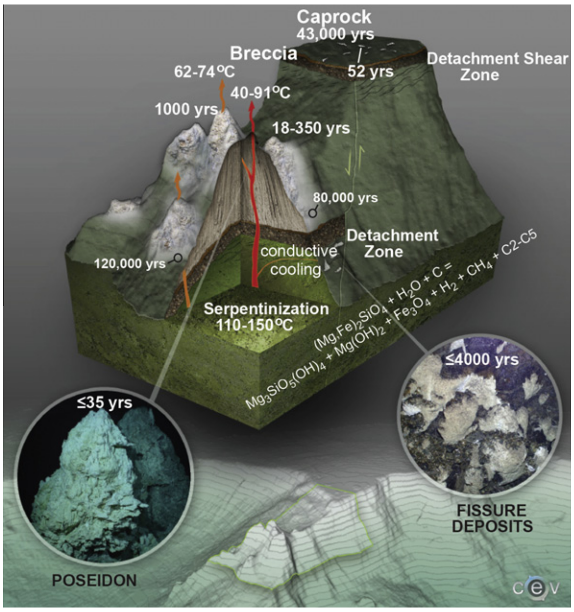

Fig. 11. Schematic of fluid flow and faulting within the Atlantis Massif. Fluid flow within the Atlantis Massif is facilitated steeply-dipping normal faults and the Poseidon complex within the LCHF marks the intersection of two primary faults which focus flow. The bathymetry of Atlantis Massif is shown at the bottom of the image and the area outlined in green has been amplified to schematically show focused flow beneath Poseidon and the ages of several of the structures within the field. Fissure deposits that form from cracks in the serpentinite rock on the East Wall of the massif vent at lower temperatures, indicating that fluids are conductively cooled during horizontal flow along cracks and fissures within the detachment shear zone.

The development of the W–E trending fault system may have been coincident with, or predated the initiation of venting through the cap rock (where ages range from 44.1 ± 3.3 to 67.4 ± 8.7 kyrs) (Table 2). However, it is important to note that the high ^{232}Th and variable $\delta^{234}U_{initial}$ values of these samples show that the cap rock has experienced significant diagenesis (Table 2 and Fig. 6b, c). The ages of three carbonate deposits that have formed within cracks in the cap rock range from 52 ± 13 to 1061 ± 844 yrs, indicating that cracking and faulting through the cap rock is very young just inboard of the steep southern wall of the massif (Table 2 and Fig. 10). Direct dive observations and high resolution bathymetry show that extreme mass wasting has occurred along the south face of the Atlantis Massif. It is likely that this process results in breaking up the cap rock and in the northward migration of the wall such that venting sites in this region are not long-lived.

In contrast to the wide range of chimney ages found on the W–E lineament, all of the samples analyzed from the near-vertical East Wall are <4 kyrs old (Figs. 2 and 10). The unique morphology of the East Wall deposits (Fig. EA-1e) is the result of gently west-dipping faults channeling sub-horizontal flow (Kelley et al., 2001, 2005) (Fig. 11). This type of fluid flow is consistent with observations made by Proskurowski et al. (2006), who showed that fluids egressing from the east side of the field have experienced conductive cooling (Fig. 11). The relatively young ages of the fissure samples collected from the East Wall indicate that this wall may have only been exposed in the last 4 kyrs. The exposure of this face is likely the result of mass wasting caused by northeasterly trending normal faults that characterize the southern face of the massif (Karson et al., 2006) (Fig. 11). These faults, coupled with expansion of the basement rocks and seismic activity result in pieces of the massif "calving off." This process creates the scalloped edges of the Atlantis Massif that are observed in extended bathymetric maps (Karson et al., 2006).

In summary, the creation of the LCHF is governed by the development of complex fault systems within the Atlantis Massif that focus hydrothermal flow. The oldest samples in the SSW portion of the field show that the formation of the W–E trending fault (Fault "A") was one of the first conduit systems for hydrothermal flow (Figs. 1 and 10). The 020° fault (Fault "B") was likely initiated at the same time (Figs. 1 and 10). Although not well constrained, it is likely that portions of these fault systems also allowed seawater to enter the crust and react with underlying peridotite. Serpentinization reactions produced warm Ca-rich, high pH fluids which rose to the surface, focused by the intersection of W-E trending and more northerly trending fault networks (Figs. 1, 10, and 11). Upon mixing with seawater, the earliest LCHF deposits began to form and gradually built on one another as fluid flow paths were sustained by a combination of seismic activity and volumetric expansion during serpentinization. Results from this study show that this process has been ongoing for at least 120 kyrs.

Schmidt et al. (2007) hypothesized that ultramafic-hosted systems on slow-spreading ridges (e.g., Logatchev, Rainbow) are longer-lived than their basalt-hosted counterparts because of the lack of frequent eruptions and dike intrusions. A similar argument can be made for the LCHF and the longevity of this system can be attributed to a combination of five factors. First, because the LCHF is located on an oceanic core complex and hosted by ultramafic rock, eruptions and dike intrusions do not disrupt the hydrology of the field, in contrast to what is typical at black smoker vent fields on fast- and intermediate-spreading ridges (e.g., Shank et al., 1998; Haymon et al., 1993; Delaney et al., 1998; Glickson et al., 2007). Second, moderate seismicity is common at the Atlantis Transform Fault, which likely promotes fracture propagation into the basement rocks and access to fresh ultramafic material (Smith et al., 2003). Third, serpentinization reactions within the massif result in volumetric expansion of the host rock, which also perpetuates cracking and opening of fluid flow paths. Fourth, fluid flow is focused by the intersection of W–E and 020° striking faults (Faults A and B in Figs. 1 and 10). This focused flow enables the long-term, continuous growth of chimney deposits to 60 m in height. Finally, the chimneys themselves are fortified by the welding and buttresses of structures at the bases: old carbonate creates nucleation sites for the formation of new carbonate and the chimneys grow upward and outward over time to create massive edifices like the Poseidon complex.

Author's personal copy

8. CONCLUSION

In this study, U–Th dating methods were applied to hydrothermal vent fluids and carbonate chimney deposits from the LCHF, making this one of the most comprehensive geochronology studies of any venting system. Ages of the carbonate deposits range from modern to 120 kyrs. These data are coupled with direct field observations and detailed mapping and show that the intersection of long-lived faults within the Atlantis Massif plays a critical role in focusing and sustaining fluid flow. Constraining the history of hydrothermal activity at any vent field has implications for providing a better understanding of the role of the field in global heat flux, chemical change, and the evolution of biological communities. Although black smoker systems are subject to episodic events triggered by magmatic and intense seismic activity that can alter fluid flow paths, it is possible that off-axis, ultramafic-hosted systems such as the LCHF may be longer-lived because of their unique geologic setting that is seismically active, but not perturbed by magmatic activity. Although numerous studies have focused on the nature of down-flow zones in black smoker systems, characterization of these systems in ultramafic environments remains an important goal for future research.

ACKNOWLEDGMENTS

The authors greatly appreciate the help of our colleagues and ship crews during the 2003 expedition to the LCHF on board the *R/V Atlantis* and the 2005 expedition on the *R/V Brown*. The authors thank D. Butterfield for critical vent fluid samples collected from the 2003 and 2005 cruises. G. Früh-Green provided helpful discussions on LCHF geochemistry. The authors also thank J. Karson for useful discussions regarding the geology of the Atlantis Massif. The authors appreciate the work of H. Hadaway and M. Stoermer at the UW Center for Environmental Visualization on one of the figures. K.A.L. thanks S. Dasgupta for helpful science conversations and L. Hill and T. Jensen for logistical support while working at UM. This work was funded by NSF Grant OCE0137206 and NOAA Ocean Exploration support to D.S. Kelley and NSC Grants 96-2116-M002-003, 97-2752-M004-PAE, and 98-2611-M002-006 to C.-C. Shen.

APPENDIX A. SUPPLEMENTARY DATA

Supplementary data associated with this article can be found, in the online version, at doi:10.1016/j.gca.2011.01.008.

REFERENCES

Allen D. E. and Seyfried W. E. (2004) Serpentinization and heat generation: constraints from Lost City and Rainbow hydrothermal systems. *Geochim. Cosmochim. Acta* **68**, 1347–1354.

Andersen M. B., Stirling C. H., Potter E.-K., Halliday A. N., Blake S. G., McCulloch M. T., Ayling B. F. and O'Leary M. (2008) High-precision U-series measurements of more than 500,000 year old fossil corals. *Earth Planet. Sci. Lett.* **265**, 229–245.

Andersen M. B., Stirling C. H., Zimmermann B. and Halliday A. N. (2010) Precise determination of the open-ocean ^{234}U/^{238}U composition. *Geochem. Geophys. Geosys.* doi:10.1029/2010GC003318.

Anderson R. F., Bacon M. P. and Brewer P. G. (1982) Elevated concentrations of actinides in Mono Lake. *Science* **216**, 514–516.

Bacon M. P. and Anderson R. F. (1982) Distribution of thorium isotopes between dissolved and particulate forms in the deep sea. *J. Geophys. Res.* **87**(C3), 2045–2056.

Blackman D. K., Cann J. R., Janssen B. and Smith D. K. (1998) Origin of extensional core complexes: evidence from the Mid-Atlantic Ridge at Atlantis Fracture Zone. *J. Geophys. Res.* **103**, 21315–21333.

Blackman D. K., Karson J. A., Kelley D. S., Cann J. R., Früh-Green G. L., Gee J. S., Hurst S. D., John B. E., Morgan J., Nooner S. L., Ross D. K., Schroeder T. J. and Williams E. A. (2002) Geology of the Atlantis Massif (Mid-Atlantic Ridge, 30°N): implications for the evolution of an ultramafic oceanic core complex. *Mar. Geophys. Res. Lett.* **23**, 443–469.

Boschi C., Früh-Green G., Delacour A., Karson J. A. and Kelley D. S. (2006) Mass transfer and fluid flow during detachment faulting and development of an oceanic core complex, Atlantis Massif (MAR 30°N). *Geochem. Geophys. Geosys.* **7**(Q01004), 1–39.

Branchu E. P., Hillaire-Marcel C., Deschamps P., Ghaleb B. and Sinclair D. J. (2005) Early diagenesis impact on precise U-series dating of deep sea corals: example of a 100–200-year old Lophelia pertusa sample from the northeast Atlantic. *Geochim. Cosmochim. Acta* **69**, 4865–4879.

Brazelton W. J., Schrenk M. O., Kelley D. S. and Baross J. A. (2006) Methane- and sulfur-metabolizing microbial communities dominate the Lost City hydrothermal field ecosystem. *Appl. Environ. Microb.* **72**, 6257–6270.

Brazelton W. J., Ludwig K. A., Sogin M. L., Andreishcheva E. N., Kelley D. S., Shen C.-C., Edwards R. L. and Baross J. A. (2010) Archaea and bacteria with surprising microdiversity show shifts in dominance over 1000-year time scales in hydrothermal chimneys. *Proc. Natl. Acad. Sci. USA* **107**, 1612–1617.

Butterfield D. A., McDuff R. E., Mottl M. J., Lilley M. D., Lupton J. E. and Massoth G. J. (1994) Gradients in the composition of hydrothermal fluids from the Endeavor Segment vent field; phase separation and brine loss. *J. Geophys. Res.* **99**, 9561–9583.

Cann J. R., Blackman D. K., Smith D. K., McAllister E., Janssen B., Mello S., Avgerinos E., Pascoe A. R. and Escartin J. (1997) Corrugated slip surfaces formed at ridge-transform intersections on the Mid-Atlantic Ridge. *Nature* **385**, 329–330.

Canales J. P., Tucholke B. E. and Collins J. A. (2004) Seismic reflection imaging of an oceanic detachment fault: Atlantis Megamullion (Mid-Atlantic Ridge, 30°N). *Earth Planet. Sci. Lett.* **222**, 543–560.

Chen J. H. and Wasserburg G. J. (1981) Isotopic determination of uranium in picomole and subpicomole quantities. *Anal. Chem.* **53**, 2060–2067.

Chen J. H., Edwards R. L. and Wasserburg G. J. (1986a) ^{238}U, ^{234}U and ^{232}Th in seawater. *Earth Planet. Sci. Lett.* **80**, 241–251.

Chen J. H., Wasserburg G. J., Von Damm K. L. and Edmond J. M. (1986b) The U–Th–Pb systematics in hot springs on the East Pacific Rise at 21°N and Guaymas Basin. *Geochim. Cosmochim. Acta* **50**, 2467–2479.

Cheng H., Edwards R. L., Murrell M. T. and Benjamin T. M. (1998) Uranium–thorium–protactinium dating systematics. *Geochim. Cosmochim. Acta* **62**, 3437–3452.

Cheng H., Adkins J., Edwards R. L. and Boyle E. A. (2000a) U–Th dating of deep-sea corals. *Geochim. Cosmochim. Acta* **64**, 2401–2416.

Author's personal copy

Cheng H., Edwards R. L., Hoff J., Gallup C. D., Richards D. A. and Asmerom Y. (2000b) The half-lives of uranium-234 and thorium-230. *Chem. Geol.* **169**, 17–33.

Cheng H., Edwards R. L., Broecker W. S., Denton G. H., Kong X., Wang Y., Zhang R. and Wang X. (2009) Ice age terminations. *Science* **326**, 248–252.

Cobb K. M., Charles C. D., Cheng H., Kastner M. and Edwards R. L. (2003) U/Th dating living and young fossil corals from the central tropical Pacific. *Earth Planet. Sci. Lett.* **219**, 91–103.

Cochran J. K. and Masqué P. (2003) Short-lived U/Th series radionuclides in the ocean: tracers for scavenging rates, export fluxes and particle dynamics. In *Uranium-series Geochemistry* (eds. S. Bourdon, G. Henderson, C. C. Lundstrom and S. P. Turner). The Mineralogical Society of America, New York, pp. 461–492.

Cutler K. B., Edwards R. L., Taylor F. W., Cheng H., Adkins J., Gallup C. D., Cutler P. M., Burr G. S. and Bloom A. L. (2003) Rapid sea-level fall and deep-ocean temperature change since the last interglacial period. *Earth Planet. Sci. Lett.* **206**, 253–271.

Delaney J. R., Kelley D. S., Lilley M. D., Butterfield D. A., Baross J. A., Wilcock W. S. D., Embley R. W. and Summit M. (1998) The quantum event of oceanic crustal accretion: impacts of diking at mid-ocean ridges. *Science* **281**, 222–230.

Dorale J. A., Edwards R. L., Alexander, Jr., E. C., Shen C.-C., Richards D. A. and Cheng H. (2001) Uranium-series dating of speleothems: current techniques, limits, and applications. In *Studies of Cave Sediments* (eds. J. Mylroie and I. D. Sasowsky). Kluwer Academic/Plenum Press, New York, pp. 1–21.

Dunk R. M., Mills R. A. and Jenkins W. J. (2002) A reevaluation of the oceanic uranium budget for the Holocene. *Chem. Geol.* **190**, 45–67.

Edwards R. L., Chen J. H. and Wasserburg G. J. (1986/1987) ^{238}U–^{234}U–^{230}Th–^{232}Th systematics and the precise measurement of time over the past 500,000 yrs. *Earth Planet. Sci. Lett.* **81**, 175–192.

Edwards R. L., Chen J. H., Ku T.-L. and Wasserburg G. J. (1987) Precise timing of the last interglacial period from mass spectrometric analysis of ^{230}Th in corals. *Science* **236**, 1537–1553.

Edwards R. L. (1988) High Precision Thorium-230 Ages of Corals and the Timing of Sea Level Fluctuations in the Late Quaternary. Ph.D. thesis, California Institute of Technology.

Edwards R. L., Gallup C. D. and Cheng H. (2003) Uranium-series dating of marine and lacustrine carbonates. In *Uranium-series Geochemistry* (eds. S. Bourdon, G. Henderson, C. C. Lundstrom and S. P. Turner). The Mineralogical Society of America, New York, pp. 363–405.

Eggins S. M., Grun R., McCulloch M. T., Pike A. W. G., Chappell J., Kinsley L., Mortimer G., Shelley M., Murray-Wallace C. V., Spotl C. and Taylor L. (2008) In situ U-series dating by laser-ablation multi-collector ICPMS: new prospects for Quaternary geochronology. *Quat. Sci. Rev.* **24**, 2523–2538.

Emmanuel S. and Berkowitz B. (2006) Suppression and stimulation of seafloor hydrothermal convection by exothermic mineral hydration. *Earth Planet. Sci. Lett.* **243**, 657–668.

Expedition Scientific Party (2005) Oceanic core complex formation, Atlantis Massif—oceanic core complex formation, Atlantis Massif, Mid-Atlantic Ridge: drilling into the footwall and hanging wall of a tectonic exposure of deep, young oceanic lithosphere to study deformation, alteration, and melt generation. *IODP Prel. Rept.*, 304. doi:10.2204/iodp.pr.304.2005.

Frohlich C., Hornbach M. J., Taylor F. W., Shen C.-C., Moala A., Morton A. E. and Kruger J. (2009) Huge erratic boulders in Tonga deposited by a prehistoric tsunami. *Geology* **37**, 131–134.

Früh-Green G. L., Kelley D. S., Bernasconi S. M., Karson J. A., Ludwig K. A., Butterfield D. A., Boschi C. and Proskurowski G. (2003) 30,000 yrs of hydrothermal activity at the Lost City vent field. *Science* **301**, 495–498.

Gallup C. D., Edwards R. L. and Johnson R. G. (1994) The timing of high sea levels over the past 200,000 yrs. *Science* **263**, 796–800.

Glickson D. A., Kelley D. S. and Delaney J. R. (2007) Geology and hydrothermal evolution of the Mothra Hydrothermal Field, Endeavor Segment, Juan de Fuca Ridge. *Geochem. Geophys. Geosys.* **8**, Q060101, doi:10.1029/2007GC001588.

Goldstein S. J. and Stirling C. H. (2003) Techniques for measuring uranium-series nuclides: 1992–2002. In *Uranium-series Geochemistry* (eds. S. Bourdon, G. Henderson, C. C. Lundstrom and S. P. Turner). The Mineralogical Society of America, New York, pp. 23–58.

Haymon R. M., Fornari D. J., VonDamm K. L., Lilley M. D., Perfit M. R., Edmond J. M., Shanks, III, W. C., Lutz R. A., Grembeier J. M., Carbotte S., Wright D., McLaughlin E., Smith M., Beedle N. and Olson E. (1993) Volcanic eruption of the mid-ocean ridge along the East Pacific Rise crest at 9°45–52′N: direct submersible observations of seafloor phenomena associated with an eruption event in April. *Earth Planet. Sci. Lett.* **119**, 85–101.

Hamelin B., Bard E., Zindler A. and Fairbanks R. G. (1991) ^{234}U/^{238}U mass spectrometry of corals: how accurate is the U–Th age of the last interglacial period? *Earth Planet. Sci. Lett.* **106**, 169–180.

Henderson G. and Anderson R. F. (2003) The U-series toolbox for paleoceanography. In *Uranium-series Geochemistry* (eds. S. Bourdon, G. Henderson, C. C. Lundstrom and S. P. Turner). The Mineralogical Society of America, New York, pp. 493–530.

Humphris S. E., Herzig P. M., Miller D. J., Alt J. C., Becker K., Brown D., Brügmann G., Chiba H., Fouquet Y., Gemmell J. B., Guerin G., Hannington M. D., Holm N. G., Honnorez J. J., Iturrino G. J., Knott R., Ludwig R., Nakamura K., Petersen S., Reysenbach A.-L., Rona P. A., Smith S., Sturz A. A., Tivey M. K. and Zhao X. (1995) The internal structure of an active seafloor massive sulphide deposit. *Nature* **377**, 713–716.

Jaffey A. H., Flynn K. F., Glendenin L. E., Bentley W. C. and Essling A. M. (1971) Precision measurement of half-lives and specific activities of ^{235}U and ^{238}U. *Phys. Rev.* **C4**, 1889–1906.

Kaufman A. and Broecker W. (1965) Comparison of ^{230}Th and ^{14}C ages for carbonate materials from Lakes Lahontan and Bonneville. *J. Geophys. Res.* **70**, 4039–4054.

Karson J. A., Früh-Green G., Kelley D. S., Williams E. A. and Yoerger D. R. (2006) Detachment shear zone of the Atlantis Massif core complex, Mid-Atlantic Ridge, 30°N. *Geochem. Geophys. Geosyst.* **7**(6), Q06016, doi:06010.01029/02005GC001109.

Kelley D. S., Karson J. A., Blackman D. K., Früh-Green G. L., Butterfield D. A., Lilley M. D., Olson E., Schrenk M. O., Roe K., Lebon G. T. and Rivissigno P.the AT3-60 Shipboard Party (2001) An off-axis hydrothermal vent field near the Mid-Atlantic Ridge at 30°N. *Nature* **412**, 145–149.

Kelley D. S., Karson J. A., Früh-Green G. L., Yoerger D., Shank T. M., Butterfield D. A., Hayes J. M., Schrenk M. O., Olson E., Proskurowski G., Jakuba M., Bradley A., Larson B., Ludwig K., Glickson D., Buckman K., Bradley A. S., Brazelton W. J., Roe K., Elend M. J., Delacour A., Bernasconi S. M., Lilley M. D., Baross J. A., Summons R. E. and Sylva S. P. (2005) A serpentinite-hosted ecosystem: the Lost City Hydrothermal Field. *Science* **307**, 1428–1434.

Kigoshi K. (1971) Alpha-recoil thorium-234; dissolution into water and the uranium-234/uranium-238 disequilibrium in nature. *Science* **173**, 47–48.

Author's personal copy

Lalou C. and Brichet E. (1982) Ages and implications of East Pacific Rise sulphide deposits at 21°N. *Nature* **300**, 169–171.

Lalou C., Reyss J. L., Brichet E., Arnold M., Thompson G., Fouquet Y. and Rona P. A. (1993) New age data for a Mid-Atlantic Ridge hydrothermal sites: TAG and Snakepit chronology revisited. *J. Geophys. Res.* **98**, 9705–9713.

Lalou C., Reyss J. L., Brichet E., Krasnov S. G., Stepanova T., Cherkashev G. A. and Markov V. F. (1996) Initial chronology of a recently discovered hydrothermal field at 14 45°N, Mid-Atlantic Ridge. *Earth Planet. Sci. Lett.* **144**, 483–490.

Lalou C., Munch U., Halbach P. and Reyss J. L. (1998a) Radiochronological investigation of hydrothermal deposits from the MESO zone, Central Indian Ridge. *Mar. Geol.* **149**, 243–254.

Lalou C., Reyss J. L. and Brichet E. (1998b) Age of sub-bottom sulfide samples at the TAG active mound. In *Proceedings of the Ocean Drilling Program, Scientific Results*, vol. 158 (ed. P. M. Herzig et al.). Ocean Drilling Program, College Station, pp. 111–117.

Lowell R. P. and Rona P. A. (2002) Seafloor hydrothermal systems driven by the serpentinization of peridotite. *Geophys. Res. Lett.* **29**(11), 21–26.

Ludwig K. A., Kelley D. S., Butterfield D. A., Nelson B. K. and Früh-Green G. L. (2006) Formation and evolution of carbonate chimneys at the Lost City Hydrothermal Field. *Geochim.Cosmochim. Acta* **70**, 3625–3645.

Ludwig K. R. (2003) Mathematical–statistical treatment of data and errors for ^{230}Th/U geochronology. In *Uranium-series Geochemistry*, vol. 52 (eds. S. Bourdon, G. Henderson, C. C. Lundstrom and S. P. Turner). The Mineralogical Society of America, pp. 631–656.

Ludwig K. R. and Titterington D. M. (1994) Calculation of ^{230}Th/U isochrons, ages, and errors. *Geochim. Cosmochim. Acta* **58**, 5031–5042.

Macdonald A. H. and Fyfe W. S. (1985) Rate of serpentinization in seafloor environments. *Tectonophysics* **116**, 123–135.

Michard A. and Albarede F. (1985) Hydrothermal uranium update at ridge crests. *Nature* **317**, 244–246.

Moran S. B., Charette M. A., Hoff J. A., Edwards R. L. and Landing W. M. (1997) Distribution of ^{230}Th in the Labrador Sea and its relation to ventilation. *Earth Planet. Sci. Lett.* **150**, 151–160.

Moran S. B., Shen C.-C., Edmonds H. N., Weinstein S. E., Smith J. N. and Edwards R. L. (2002) Dissolved and particulate ^{231}Pa and ^{230}Th in the Atlantic Ocean: constraints on intermediate/deep water age, boundary scavenging, and ^{231}Pa/^{230}Th fractionation. *Earth Planet. Sci. Lett.* **203**, 999–1014.

Mottl M. J. and Wheat G. C. (1994) Hydrothermal circulation through mid-ocean ridge flanks: fluxes of heat and magnesium. *Geochim. Cosmochim. Acta* **58**, 2225–2237.

Münch U., Lalou C., Halbach P. and Fujimoto H. (2001) Relict hydrothermal events along the super-slow Southwest Indian spreading ridge near 63 degrees 56′E—mineralogy, chemistry, and chronology of sulfide samples. *Chem. Geol.* **177**, 341–349.

Potter E. K., Stirling C. H., Wiechert U. H., Halliday A. N. and Spotl C. (2005) Uranium-series dating of corals in situ using laser-ablation MC-ICPMS. *Int. J. Mass Spectrom.* **240**, 27–35.

Proskurowski G., Lilley M. D., Kelley D. S. and Olson E. J. (2006) Low temperature volatile production at the Lost City Hydrothermal Field, evidence from a hydrogen stable isotope geothermometer. *Chem. Geol.* **229**, 331–343.

Proskurowski G., Lilley M. D., Seewald J. S., Früh-Green G. L., Olson E. J., Lupton J. E., Silva S. P. and Kelley D. S. (2008) Abiogenic hydrocarbon production at the Lost City Hydrothermal Field. *Science* **319**, 604–607.

Robinson L. F., Belshaw N. B. and Henderson G. M. (2004) U and Th concentrations and isotope ratios in modern carbonates and waters from the Bahamas. *Geochim. Cosmochim. Acta* **68**, 1777–1789.

Schmidt K., Koschinsky A., Garbe-Schönberg D., de Carvalho L. M. and Seifert R. (2007) Geochemistry of hydrothermal fluids from the ultramafic-hosted Logatchev hydrothermal field, 15°N on the Mid-Atlantic Ridge: Temporal and spatial investigation. *Chem. Geol.* **242**, 1–21.

Schrenk M. O., Kelley D. S., Bolton S. A. and Baross J. A. (2003) Low archaeal diversity linked to subseafloor geochemical processes at the Lost City hydrothermal field. *Environ. Microbiol.* **6**, 1086–1095.

Schroeder T. and John B. E. (2004) Strain localization on an oceanic detachment fault system, Atlantis Massif, 30°N, Mid-Atlantic Ridge. *Geochem. Geophys. Geosys.* **5**, doi:10.1029/2004GC000728.

Shank T. M., Fornari D. J., Von Damm K. L., Lilley M. D., Haymon R. M. and Lutz R. A. (1998) Temporal and spatial patterns of biological community development at nascent deep-sea hydrothermal vents (9°50′N, East Pacific Rise). *Deep-Sea Res. II* **45**, 465–515.

Shen C.-C., Edwards R. L., Cheng H., Dorale J. A., Thomas R. B., Moran S. B., Weinstein S. E. and Edmonds H. N. (2002) Uranium and thorium isotopic and concentration measurements by magnetic sector inductively coupled plasma mass spectrometry. *Chem. Geol.* **185**, 165–178.

Shen C.-C., Cheng H., Edwards R. L., Moran S. B., Edmonds H. N., Hoff J. A. and Thomas R. B. (2003) Measurement of attogram quantities of ^{231}Pa in dissolved and particulate fractions of seawater by isotope dilution thermal ionization mass spectrometry. *Anal. Chem.* **75**, 1075–1079.

Shen C.-C., Lin H.-T., Chu M.-F., Yu E.-F., Wang X. and Dorale J. A. (2006) Measurement of natural uranium concentration and isotopic composition with permil-level precision by inductively coupled plasma quadrupole mass spectrometry. *Geochem. Geophys. Geosyst.* **7**, Q09005, doi:10.1029/2006GC001303.

Shen C.-C., Li K.-S., Sieh K., Natawidjaja D., Cheng H., Wang X., Edwards R. L., Lam D. D., Hsieh Y.-T., Fan T.-Y., Melzner A., Taylor F. W., Quinn T. M., Chiang H.-W. and Kilbourne K. H. (2008) Variation of initial ^{230}Th/^{232}Th and limits of high precision U–Th dating of shallow-water corals. *Geochim. Cosmochim. Acta* **72**, 4201–4223.

Shen C.-C., Kano A., Hori M., Lin K., Chiu T.-C. and Burr G. S. (2010) East Asian monsoon evolution and reconciliation of climate records from Japan and Greenland during the last deglaciation. *Quat. Sci. Rev.* **29**, 3327–3335.

Simpson H. J., Trier R. M., Toggweiler J. R., Mathieu G., Deck B. L., Olsen C. R., Hammond D. E., Fuller C. and Ku T.-L. (1982) Radionuclides in Mono Lake, California. *Science* **216**, 512–514.

Smith D. K., Escartin J., Cannat M., Tolstoy M., Fox C. G., Bohnenstiehl D. R. and Bazin S. (2003) Spatial and temporal distribution of seismicity along the northern Mid-Atlantic Ridge (15–35°N). *J. Geophys. Res.* **108**, 31.

Stirling C. H., Esat T. M., Lambeck K., McCulloch M. T., Blake S. G., Lee D. C. and Halliday A. N. (2001) Orbital forcing of the marine isotope stage 9 interglacial. *Science* **291**, 290–293.

Stirling C. H. and Andersen M. B. (2009) Uranium-series dating of fossil coral reefs: extending the sea-level record beyond the last glacial cycle. *Earth Planet. Sci. Lett.* **284**, 269–283.

Taylor S. R. and McLennan S. M. (1985) *The Continental Crust: Its Composition and Evolution*. Blackwell, Oxford.

Taylor S. R. and McLennan S. M. (1995) The geochemical evolution of the continental crust. *Rev. Geophys.* **33**, 241–265.

Author's personal copy

Thompson W. G., Spiegelman M. W., Goldstein S. L. and Speed R. C. (2003) An open-system model for U-series age determinations of fossil corals. *Earth Planet. Sci. Lett.* **210**, 365–381.

Villemant B. and Feuillet N. (2003) Dating open systems by the ^{238}U–^{234}U-^{230}Th method: application to Quaternary reef terraces. *Earth Planet. Sci. Lett.* **210**, 105–118.

Voltaggio M., Tuccimei P., Branca M. and Romoli L. (1998) U-series disequilibrium radionuclides in sulphur incrustations from the fumarolic field of Vulcano Island. *Geochim. Cosmochim. Acta* **62**, 2111–2127.

You C.-F. and Bickle M. J. (1998) Evolution of an active seafloor massive sulphide deposit. *Nature* **394**, 668–671.

Associate editor: Miryam Bar-Matthews